Using flow cytometry and light-induced fluorescence technique to characterize the variability and characteristics of bioaerosols in springtime at Metro Atlanta, Georgia

Arnaldo Negron[a,b], Natasha DeLeon-Rodriguez[c$], Samantha M. Waters[a#], Luke D. Ziemba[d], Bruce Anderson[d], Michael Bergin[e], Konstantinos T. Konstantinidis[f,c*], and Athanasios Nenes[a,g,h*]

[a] School of Earth and Atmospheric Sciences, Georgia Institute of Technology, Atlanta, GA 30332, USA
[b] School of Chemical and Biomolecular Engineering, Georgia Institute of Technology, Atlanta, GA 30332, USA
[c] School of Biology, Georgia Institute of Technology, Atlanta, GA 30332, USA
[d] Chemistry and Dynamics Branch/Science Directorate, National Aeronautics and Space Administration Langley Research Center, Hampton, VA 23681, USA
[e] Department of Civil and Environmental Engineering, Duke University, Durham, NC, 2770, USA
[f] School of Civil and Environmental Engineering, Georgia Institute of Technology, Atlanta, GA 30332, USA
[g] Institute for Chemical Engineering Science, Foundation for Research and Technology Hellas, Patra, GR-26504, Greece
[h] Laboratory of Atmospheric Processes and their Impacts (LAPI), School of Architecture, Civil & Environmental Engineering, Ecole Polytechnique Fédérale de Lausanne, CH-1015, Switzerland
[$] Currently at: Puerto Rico Science, Technology and Research Trust, Rio Piedras, 00927, Puerto Rico
[#] Currently at: Department of Marine Sciences, University of Georgia, Athens, GA 30602-3636
*Corresponding Author

Abstract

The abundance and speciation of primary biological aerosol particles (PBAP) is important for understanding their impacts on human health, cloud formation and ecosystems. Towards this, we have developed a protocol for quantifying PBAP collected from large volumes of air with a portable wet-walled cyclone bioaerosol sampler. A flow cytometry (FCM) protocol was then developed to quantify and characterize the PBAP populations from the sampler, which were confirmed against epifluorescence microscopy. The sampling system and FCM analysis were used to study PBAP in Atlanta, GA over a two-month period and showed clearly defined populations of nucleic acid containing particles: Low Nucleic Acid-content particles above threshold (LNA-AT), and High Nucleic Acid-content particles (HNA) likely containing wet-ejected fungal spores, and pollen. We find that daily-average springtime PBAP concentration (1 to 5μm diameter) ranged between 1.4×10^4 and 1.1×10^5 m^{-3}. The LNA-AT population dominated PBAP during dry days (72 ± 18%); HNA dominated the PBAP during humid days and following rain events, where HNA comprised up to 92% of the PBAP number. Concurrent measurements with a Wideband Integrated Bioaerosol Sensor (WIBS-4A) showed that FBAP and total FCM counts are similar;

HNA (from FCM) moderately correlated with ABC type FBAP concentrations throughout the sampling period (and for the same particle size range, 1-5 μm diameter). However, the FCM LNA-AT population, possibly containing bacterial cells, did not correlate with any FBAP type. The lack of correlation of any WIBS FBAP type with the LNA-AT suggest airborne bacterial cells may be more difficult to unambiguously detect with autofluorescence than currently thought. Identification of bacterial cells even in the FCM (LNA-AT population) is challenging, given that the fluorescence level of stained cells at times may be comparable to that seen from abiotic particles. HNA and ABC displayed highest concentration on a humid and warm day after a rain event (4/14), suggesting that both populations correspond to wet-ejected fungal spores. Overall, information from both instruments combined reveals a highly dynamic airborne bioaerosol community over Atlanta, with a considerable presence of fungal spores during humid days, and LNA-AT population dominating bioaerosol community during dry days.

Introduction

Primary biological aerosol particles (PBAP), also called bioaerosols, are comprised of airborne microbial cells (e.g. bacteria, diatoms), reproductive entities (e.g. pollen, fungal spores), viruses and biological fragments. Bioaerosols are ubiquitous, with potentially important impacts on human health, cloud formation, precipitation, and biogeochemical cycles (Pöschl, 2005; Hoose et al., 2010; DeLeon-Rodriguez et al., 2013; Morris et al., 2014; Longo et al., 2014; Fröhlich-Nowoisky et al., 2016; Myriokefalitakis et al., 2016). Despite their low number concentration relative to abiotic particles, PBAP possess unique functional and compositional characteristics that differentiate them from abiotic aerosol. For example, certain PBAP constitute the most efficient of atmospheric ice nucleators, affecting the microphysics of mixed phase clouds and precipitation (Hoose and Möhler, 2012; Sullivan et al., 2017). The mass and nutrient content of PBAP may suffice to comprise an important supply of bioavailable P to oligotrophic marine ecosystems (Longo et al., 2014; Myriokefalitakis et al., 2016). In addition, the concurrence of disease outbreaks during dust storms has been attributed to pathogenic microbes attached to airborne dust that are subsequently inhaled (Griffin et al., 2003; Ortiz-Martinez et al., 2015; Goudie 2014).

Quantification of the concentration and size of PBAP is critical for understanding their environmental impacts. Measuring PBAP however poses a challenge for established microbiology tools, owing to their low atmospheric concentration (10^3 - 10^6 cells m^{-3} air; Fröhlich-Nowoisky et al., 2016) and wide diversity of airborne particle types and sizes. For instance, only a fraction of microorganisms (an estimated 5%; Chi and Li et al., 2007) can be cultured, and cultivation cannot be used to quantify dead organisms, viruses or fragments, while most culture-independent methods are optimized for more abundant microbial populations. Epifluorescence microscopy (EPM) is the standard for bioaerosol quantification but is not

high-throughput and requires considerable time for quantification of concentration per sample. Flow cytometry (FCM) is an analysis technique based on the concurrent measurement of light scattering and fluorescence intensity from single particles (Wang et al., 2010). FCM requires a liquid suspension of bioparticles that flows through an optical cell and interrogated with a series of laser beams. Each sample is pretreated with stains that targeting specific macromolecules (e.g. DNA/RNA) which subsequently fluoresce when excited by the FCM lasers. The resulting scattering and fluorescent light emissions are then detected by an array of sensors to allow the differentiation of biological and abiotic (e.g. dust) particles according to the characteristic specific to the stain used. FCM has proved to be as reliable as EPM, but with the advantage of lower uncertainty, higher quantification efficiency and requiring considerably less time and effort than EPM per sample (Lange et al., 1997). FCM is frequently used in biomedical research to quantify eukaryotic cell populations, and in microbiology to quantify a wide variety of yeast and bacterial cells (Nir et al., 1990; Van Dilla et al., 1983). FCM is also used to study environmental samples, e.g., to differentiate low nucleic acid (LNA) from high nucleic acid (HNA) phytoplankton in aquatic environments (Wang Y. et al 2010; Müller et al., 2010). Despite its advantages, FCM has seen little use in the bioaerosol field to date, owing in part to the challenges associated with collecting sufficient PBAP mass for robust counting statistics to be obtained (Chen and Li, 2005; Liang et al., 2013). Chen and Li (2005) determined that for counting purposes, the SYTO-13 nucleic acid stain is the most effective (among five different nucleic acid stains studied) for determining reliable concentration of bioaerosols.

Light Induced Fluorescence (LIF) is an increasingly utilized technique for bioaerosol quantification, and it relies on measuring the autofluorescence intensity of specific high yield fluorophores (e.g., Nicotinamide Adenine Dinucleotide – NADH co-enzyme, flavins and amino acids like Tryptophan and Tyrosine) present in PBAP. The major advantage of the technique is that it is fully automated, does not require a liquid suspension (i.e., it directly senses particles suspended in air) and it provides high frequency measurements (~1 Hz) make it ideal for continuous monitoring and operation in highly variable environments (e.g., aircraft operation). Particles detected by LIF, called Fluorescent Biological Aerosol Particles (FBAP), although not equal to PBAP, may still constitute a large fraction of the biological particles (Healy et al., 2014; Gosselin et al., 2016). Using LIF, FBAP diurnal cycles showing maximum concentrations during evenings and minimum around middays, especially in heavily vegetated environments have been observed. This behavior has been related to known temperature and relative humidity release mechanism of certain fungal spore species (Wu et al., 2007; Gabey et al., 2010; Tropak and Schnaiter, 2013). Huffman et al. (2010) used a UV-Aerodynamic Particle Sizer (UV-APS) to show that the concentration and frequency of occurrence of 3μm FBAP particles at Mainz, Germany (semi-urban environment) exhibited a strong diurnal cycle from August through November: with a first peak at ~ 1.6×10^4 m^{-3} at mid-morning (6-8 am) followed by a constant profile (~ $2\text{-}4\times10^4$ m^3) throughout the rest of

the day. Similar studies in urban and densely vegetated environments suggest a notable difference in the size distributions, diurnal behavior and FBAP loading between the two environments. Gabey et al., 2011 found that the FBAP in Manchester, UK follow a characteristic bimodal distribution with peaks at 1.2µm and 1.5 – 3.0 µm. As in Mainz, the concentration of larger particles peaks in the mid-morning, ranges from 0 to 300 L^{-1}, and the 1.2µm peak is linked to traffic activity. However, at the Borneo tropical rain forest FBAP concentrations peak during the evening with a robust 2-3µm population and concentrations ranging from 100 to 2000 L^{-1} (Gabey et al., 2010).

LIF-based observations (e.g. UV-APS, WIBS), combined with measurements of molecular tracers (e.g. mannitol and arabitol) and endotoxin measurements provide a more complete picture of PBAP emissions. Gosselin et al. (2016) applied this approach during the BEACHON-RoMBAS field campaign. A clear correlation between FBAP and the molecular markers is seen, indicating an increase of fungal spores during rain events. FBAP concentrations and molecular marker-inferred (arabitol and mannitol; Bauer et al., 2008 approach) fungal spore concentrations were within the same order of magnitude. WIBS-3 cluster (determined using Crawford et al., 2015) linked to fungal spores gave concentrations 13% lower than those derived from molecular marker concentrations during rain events. During dry events, FBAP and molecular markers derived fungal spore concentrations were poorly correlated. It is currently unknown the degree to which all types of PBAP are consistently detected by LIF over different time of the year and different environments; it is likely, however, that for certain classes of bioparticles (e.g., pollen and fungi) the detection efficiency using LIF is relatively high. However, the low intrinsic fluorescence intensity of bacteria and high variability of thereof in relation to metabolic state may lead to their misclassification as non-biological particles (Hernandez et al., 2016).

For LIF-based quantification of PBAP to be effective, it requires the intrinsic fluorescence of biological material to exceed that of non-biological matter. Depending on the type, metabolic state and species, PBAP autofluorescence may vary orders of magnitude and therefore LIF may not always be able to differentiate between biological and abiotic particles. For example, Tropak and Schnaiter (2013) showed that laboratory-generated mineral dust, soot and ammonium sulfate may be misclassified as FBAP. To address misclassification, Excitation Emission Matrices (EEMs) have been developed for biomolecules (e.g. tryptophan, tyrosine, riboflavin) and non-biological (e.g. Pyrene, Naphthalene, Humic Acid) molecules. EEMs provide the wavelength-dependent fluorescence emission spectra as a function of the excitation wavelength and are used to assign spectral modes to known fluorophores. The structure of EEMs is important for identifying molecules that are unique to PBAP and allow their identification by LIF; it is this principle upon which detectors in commercial FBAP measurements (e.g. WIBS, UV-APS) are based upon. Comparison of EEMs from biological and non-biological molecules show that even when biomolecules

have higher autofluorescence intensity than non-biologicals in the LIF detection range, interferences from non-biological compounds (e.g. polycyclic aromatic hydrocarbons and soot) from combustion emissions can influence LIF detection (Pöhlker et al., 2012). Considerable work remains on determining which detector(s) or combination thereof provides an unambiguous identification of bioaerosols and related subgroups (e.g. bacteria, fungal spores, pollen). Towards this, an aerobiology catalog of pure cultures has been developed for the WIBS-4 showing that instrument-to-instrument variability in fluorescence detection poses a considerable challenge, as applying common detection thresholds across instruments leads to considerable differences in PBAP concentration and composition (Hernandez et al., 2016).

Another important issue for LIF-based quantification of PBAP is the impact of atmospheric oxidants, UV and other stressors on the fluorescence intensity of PBAP. Pan et al. (2014) tested the effect of relative humidity and ozone exposure in the autofluorescence spectra of octapeptide aerosol particles using an UV-APS connected to a rotating drum. Octapeptides, organic molecules containing eight amino acids and present in cells, were used as a proxy to study the aging of tryptophan and results suggest bioaerosols exposure to typical ozone (~150ppb) concentrations decrease tryptophan fluorescence intensity and PBAP detection. Multiple stressors can be affecting bioaerosols LIF detection so such issues need to be thoroughly explored to undersand PBAP detection efficiency over the wide range of atmospheric conditions and PBAP population composition (Toprak and Schnaiter, 2013; Hernandez et al., 2016).

The aims of the study are to (i) develop an effective and reliable FCM detection and quantification protocol for bioaerosol; (ii) apply the protocol to understand bioaerosol populations and their variability during different meteorological conditions, and, (iii) compare FCM and WIBS-4A results to have a better understanding of PBAP day-to-day variability. To our knowledge, this study is the first to develop a FCM protocol to identify and quantify well-defined speciated bioaerosols populations from samples collected from a modified state-of-the-art biosampler. LIF sampling of bioaerosol side-by-side with established and quantitative biology tools (FCM and EPM) was conducted to assess the LIF detection capabilities toward different bioaerosol populations and under atmospherically-relevant conditions during this study. Atlanta is selected as a case study for PBAP sampling, as it provides a highly populated urban environment surrounded by vast vegetative areas; this and the broad range of temperature and humidity ensures a wide range of PBAP population composition, state and concentrations. All the samples collected are compared side-by-side to concurrent WIBS-4A data collected over the same time period.

2. Instrumentation and Methodology

2.1 Bioaerosol Sampler

Sampling was performed using the SpinCon II (InnovaPrep LLC, Inc.) portable wet-walled cyclone aerosol sampler. Aerosol is collected by inertial impaction with a recirculating liquid film in the cyclone; evaporative losses are compensated so that the sample volume is maintained constant during a sample cycle. The particle collection efficiency for 1µm, 3µm, 3.5µm and 5.0µm particles is about 47.3±2.1%, 56.1±3.9%, 14.6 ± 0.6 and 13.8 ± 2.2%, respectively (Kesavan et al., 2015). However, the experiments conducted using 1µm PSL and 3µm PSL, 3.5µm oleic acid and 5.0µm oleic acid particles not necessarily quantify the collection efficiency of biological particles in this size range. Even with a lower collection efficiency than any impingement sampler, SpinCon effectively collects larger amounts of biological particles owing to its high volumetric flow rate, which is a considerable advantage (Kesavan et al., 2015). However, the stress caused by the high flow rate of the SpinCon may affect cell viability. Santl-Temkiv et al. (2017) recently studied the SpinCon retention efficiency from sea water samples and for *P.agglomerans* populations from pure cultures (~ 10^5 cells mL^{-1}). After 1 hour of sampling, the SpinCon was found to retain 20.6±5.8% of the *P.agglomerans* concentration and 55.3±2.1% of the sea water microbial concentration.

In our study, the biosampler was run at 478L min^{-1} for 4hr sampling cycles. Phosphate-buffered saline (PBS) 1X pH 7.4 solution was used and the instrument compensated for water evaporation by supplying Milli-Q water to maintain the PBS concentration constant. Upon termination of each sampling cycle, the instrument was programmed to dispense the sample in a 15mL centrifuge tube. Then, 10µl of formalin (37 wt.% formaldehyde) per mL of solution was added to every sample for preservation and samples were stored at 4°C. Given the long sampling times and the low concentration of PBAP, the fluid supply system of the instrument was modified and a cleaning protocol (CP) has been developed, which is described below.

The SpinCon II water and PBS supply bags used in the commercial instrument were replaced by two 2L autoclavable Nalgene bottles (Thermo Scientific Inc.) with antimicrobial tubing, connectors and a small HEPA filter connected to vent and prevent coarse and submicron particles contamination (Figure 1). Bottles were autoclaved and filled with Milli-Q water and PBS, beforehand sterilized with 0.2µm pore bottle top filters (Thermo Fisher Inc.) and transferred inside a biosafety cabinet. An aliquot of each fluid obtained after preparation was evaluated for sterility by EPM and FCM.

The cleaning protocol (CP) of the biosampling system consists of two phases. During phase one, all acrylic windows and the outside of the collector/concentrator were cleaned with ethanol 70 wt. %. Then, the instrument inlet, outlet, and the inside of the collector/concentrator was cleaned with ethanol 70 wt. %. In the second phase, the SpinCon II inlet was connected to a HEPA filter to provide a particle-free source

of air to the sampling system; the instrument was then washed with ethanol 70 wt.%, 10 wt.% bleach solution, PBS and Milli-Q H_2O, respectively. The wash consisted of a rinse, a 2 minutes sample and filling the instrument collector/concentrator with the fluid in use (i.e., bleach solution, ethanol, PBS and Milli-Q H_2O). The collector/concentrator was drained after 1 minute. The above were repeated for the remaining fluids, taking 5 minutes per fluid. Overall, the CP requires 45 minutes; upon completion, a blank is obtained to constrain the residual contamination levels after cleaning (described below). Finally, the HEPA filter was disconnected, instrument inlets and outlets were sealed and the inlet tube was cleaned with ethanol 70 wt.% to be ready for rooftop sampling. SpinCon II was rinsed with ethanol 70wt.% after each sampling episode and the cleaning protocol was applied before each sample.

Several blanks were obtained to quantify the levels of PBAP contamination in the fluids and sampler, and to ensure that they were sufficiently low to not bias the detection, identification and quantification of the PBAP. Furthermore, an instrument blank was obtained after a CP to constrain residual particles, by running the sampler for 2 minutes, while sampling air with a HEPA filter connected to the inlet of the SpinCon II. Another blank was collected to characterize any contamination of biological particles from the supply of PBS and water in the SpinCon II. This was done by operating the SpinCon II for a 4hr period with a HEPA filter connected to the inlet which completely cleans the air entering the wet cyclone from any bioparticles. All blanks were analyzed directly via FCM (Sect. 2.3) and EPM.

The volumetric flow rate within the SpinCon II was routinely calibrated by a VT100 Hotwire Thermo-anemometer (Cole Palmer Inc.) using a 3-hole round duct transverse approach. A 1 ¼" OD tube with the same diameter as the SpinCon II inlet was designed with 3 holes. Each hole was 60° apart from the other and the holes were perpendicular to the axial air flow direction of the tube. (Supplementary Information, Figure S1). Triplicates of flow rate measurements were taken in each hole at the center of the tube and averaged to determine SpinCon II volumetric flow rate (478.0 ± 6.4 L min^{-1}).

2.2 Flow Cytometry

During this study, a BD Accuri C6 flow cytometer (BD Bioscience Inc.) was used for Flow Cytometry. The instrument quantifies suspended cells in aqueous medium at three flow velocity modes (slow, medium and fast flow at 14, 35 and 66 µL min^{-1}, respectively). It excites particles with a 488nm laser and possesses four fluorescence detectors: FL1 (533±30nm), FL2 (585±40nm), FL3 (> 670nm) and FL4 (675±25nm), which make it possible to analyze the fluorescence from multiple dyes concurrently. In this study, 2.5 µM SYTO-13 nucleic acid probe was added to the fixed samples and incubated for 15min in the dark at room temperature to stain biological particles. Additionally, 10µL of 15µm polystyrene bead suspension was added to the 1mL total volume samples as an internal standard for PBAP concentration and size quantification. The BD Accuri C6 was cleansed before each use with 0.2µm filtered Milli-Q water in fast

mode for 10min; background particle counts were typically reduced to $1\mu L^{-1}$. At the beginning of every experiment, a 1mL blank of the atmospheric sample without SYTO-13 and beads was analyzed, used in quantification calculations (Sect. 3.1). Each sample was run in slow mode for 5min. After each sample, the instrument was flushed with 0.2µm filtered Milli-Q water in slow flow for 1 minute (important for robust quantification of the typically low concentrations of the atmospheric samples). SYTO-13 fluorescence intensity was quantified by the FL1-A detector and used in combination with other parameters (FSC-A & SSC-A) to constrain the PBAP populations present. FSC-A measured forward (0° ± 13°) scattering and is used to characterize the size of particles; SSC-A measured the side (90° ± 13°) scattering and is used to characterize the internal complexity of particles. The SSC-A scattering intensity is a function of the cellular granularity or density of the internal structures (e.g. nucleus, mitochondria, ribosomes), the sphericity and size of the particles. Compared to spherical particles of the same size, elongated particles tend to yield a broader distribution of side scattering intensities (Mage et al., 2019; Mathaes et al., 2013). Although side scattering intensity increases with particle size, it has not been commonly used to measure cell size (Tzur et al., 2011). Overall, SSC-A scattering intensity will be proportional to the amount scattering caused by the internal structures and the cell membrane, which ultimately depends on the refractive index of each cell (Muller et al., 2010). Side scattering has been effective to distinguish cells of different complexities (e.g. monocytes and granulocytes; Shapiro, 2005).

A 80,000 unit intensity FSC-H threshold (default FSC-H threshold value suggested by the manufacturer to minimize the effect of noise) was set in the instrument during data acquisition to minimize the effects of noise on bioparticle counts. The FSC-H channel (where H denotes height), measures single-particle forward scattering (FSC) intensity based on the peak (maximum point) of the voltage pulse curve recorded when a single particle goes through the interrogation point in the flow cytometer, whereas FSC-A, where A denotes area, measures single-particle FSC intensity based on the area below the curve of the recorder pulse. When the 80,000 unit FSC-H threshold is defined, only signals with an intensity greater than or equal to threshold value will be processed, and this could affect the statistics and detection efficiency of the flow cytometer toward small particles (≤ 1µm). Experiments conducted with 1.0µm polystyrene beads suspension (Supplemental information; Figure S16) have shown that 1.0µm beads have FSC-H intensities above the 80k threshold, no particle losses is observed, and beads estimated concentration agree with the reported by the manufacturer (~6×10^7 mL^{-1}; Life Technologies, Inc.) The FCM data from each sample was analyzed using the Flow Jo software (https://www.flowjo.com/solutions/flowjo) to gate and quantify bioparticles population. The same procedure was used to analyze the PBS, Milli-Q water and blanks.

2.3 LIF detection of PBAP

The WIBS-4A (referred to henceforth as "WIBS") is a single biological particle real time sensor, which measures particle light scattering and autofluorescence in an approximately 0.5 – 15µm particle range (www.dropletmeasurement.com). Particles are initially sized using the 90-degree side-scattering signal from a 635 nm continuous-wave diode laser. The scattering intensity is directly related to particle diameter and was calibrated prior to deployment using polystyrene latex sphere calibration standards (PSL with 0.8, 0.9, 1.0, 1.3, 2.0, 3.0 µm diameter, Thermo Scientific Inc.). The WIBS optical size therefore refers to PSL material with a real refractive index of 1.59. Healy et al. (2012) determined WIBS-4 counting efficiency by aerosolizing standardized concentrations of PSL sphere of specific sizes (e.g. 0.3, 0.4, 0.56, 0.7, 0.9 and 1.3µm) and compared WIBS-4 total counts against PSL counts detected by the condensation particle counter (CPC). Results show WIBS-4 possesses a 50% counting efficiency for 0.5µm particles and detects 100% of the PSL particles above 0.7µm when it is compared to the CPC counts. The 280nm and 370nm pulsed Xenon flashtube UV lights in the WIBS cause the particles to autofluoresce (i.e., excite the chromophores preexisting in the PBAP and do not rely on a fluorescent dye as done in FCM). Then, fluorescent emissions are measured at three wavelength channels, which following the nomenclature of Perring et al. (2015) are: (*i*) channel A ("FL1_280" in previous studies; Robinson et al., 2013), which refers to the detected emission between 310-400nm after excitation at 280nm, (*ii*) channel B ("FL2_280" in previous studies), which refers to the detected emission between 420-650nm after excitation at 280nm, and, (*iii*) channel C ("FL2_370" in previous studies), which refers to the detected emission between 420-650nm after excitation at 370nm. The resulting autofluorescence from 280nm excitation is affected by the presence of tryptophan, tyrosine and phenylalanine amino acids in the PBAP (Pöhlker et al., 2012). Similarly, the resulting autofluorescence from the 370nm excitation is influenced by the presence of riboflavin and co-enzyme Nicotinamide Adenine Dinucleotide Phosphate (NAD(P)H) within the cells.

Biological and non-biological particles can be discriminated by using a fluorescent intensity threshold; here the threshold is determined with the Gabey et al. (2010) method and with modifications by Perring et al. (2015) as follows. Particles with fluorescence intensities below the fluorescence threshold in all channels are categorized as non-fluorescent (NON-FBAP). Particles that fluoresce above the threshold in only one channel are named with a single letter (e.g. A, B or C); particles that fluoresce in two channels are named with the two channel letters (e.g. AB, AC or BC), while particles that fluoresce in all channels are categorized as type ABC. Furthermore, the total FBAP concentration is defined as the sum of the concentration in the seven FBAP categories defined above. This approach was applied by Hernandez et al., (2016) to pure culture PBAP (bacteria, fungal spores, pollen) to study their correspondence to FBAP types; bacteria tend to be detected by type A, and fungal spores and pollen by type AB and ABC. However, bioaerosol classification is instrument-specific and particle size dependent (Hernandez et al., 2016; Savage et al., 2017). Multiple environments have been studied using the Perring et al. 2015 FBAP types, including

rural, urban and highly vegetated locations. In the Southeastern US, the total FBAP concentration range from 2×10^4 to 8×10^4 m^{-3}, constituting 3-24% of the total supermicron particle number between 1 and 10μm diameter. In the highly vegetated Rocky Mountains, ABC type particles are enhanced during rainy days (during or post-rain events) to ~ 65% of the total FBAP, owing to the release of wet-ejected fungal spores following precipitation (Gosselin et al., 2016). On the contrary, in the highly populated city of Nanjing, China all FBAP types, except type C, correlated with black carbon concentrations, suggesting a strong interference by combustion sources (Yu et al., 2016). A detailed explanation of the above-mentioned studies using Perring et al. 2015 approach is also included in the section SI.20 of the supplemental information.

2.4 Location of sampling site and sampling frequency

Bioaerosol sampling was conducted between April 7 and May 15, 2015 at the rooftop sampling platform of the Ford Environmental Sciences and Technology (ES&T) building at the Georgia Institute of Technology campus in Atlanta, GA. The site, which was located at the heart of a major urban environment, is surrounded by dense forested areas in the southeastern USA: the Oconee National Forest (South East), the Chattahoochee National Forest (North), and the Talladega National Forest (West). The WIBS was operating continuously throughout the same period, sampling bioaerosol from a 15 ft. long and ¼ in. ID conductive tubing inlet fixed 8 ft. above the sampling platform floor. The SpinCon II was placed in the platform during sampling episodes with its inlet facing South. Three 4-hour samples per week were collected with the Spincon II sampler over the 5-week period (4 h sampling between 10am and 5pm; Table 1). Meteorological data acquired from the same platform provided wind speed, wind direction, relative humidity (RH), temperature, total hourly rain and UV radiation index with a 1min resolution.

3. Data processing and Analysis

3.1 FCM data processing

All blanks collected showed contamination levels that did not exceed 1% of the PBAP quantified in the subsequent atmospheric samples. The 2-minute instrument blanks obtained after the CP and the HEPA filter washes was $1.06\times10^3 \pm 7.37\times10^2$ mL^{-1} and $9.22\times10^2 \pm 1.24\times10^2$ mL^{-1}, respectively, which are negligible accumulations compared to the $2.55\times10^5 \pm 1.14\times10^5$ mL^{-1} average PBAP concentration quantified in the atmospheric samples. The concentration of PBAP in the blanks was also confirmed with microscopy (not shown). Based on this, we are confident that the CP protocol and procedure to replace the working fluids ensured sterility of the biosampler before each sampling.

FCM analysis of the samples was carried out as follows. We obtain the fluorescence intensity (from each of the 4 fluorescence detectors), forward scattering and side scattering intensity for all the particles suspended in the samples. A gating procedure was used to determine the fluorescence levels associated with detecting only particles containing SYTO-13 (hence, a PBAP) and background fluorescence from non-

stained particles. The procedure (Supplemental information, SI.2 and SI.3) consists of 3 steps: (a) fluorescence threshold determination, (b) population gating, and, (c) biological/non-biological particle discrimination in the population(s) within the threshold (e.g. LNA PBAP, Section 4.1). The fluorescence threshold was determined using an atmospheric sample without SYTO-13 collected before each FCM analysis, as a blank. Based on the fluorescence responses obtained, we determine the FL1-A fluorescence intensity value for which 99.5% or 99.9% of the (unstained) particles of the blank autofluoresce below the chosen value. This FL1-A intensity, called "fluorescence threshold", was determined for each sample (supplementary information, Figure S2a and S2b). The determination of the fluorescence threshold involved selecting the most conservative value that maximizes inclusion of biological particles and minimizes the inclusion of non-biological particles, including those that may be subject to background fluorescence or unspecific binding of SYTO-13 (Diaz et al., 2010; Müller et al., 2010). We found out that threshold values for the 99.9% approach were substantially higher than 99.5% approach in multiple sampling events and comparable to the fluorescence intensities observed for stained pure cultures (~10^5 units), which means that the 99.9% threshold values will miscount pure cultures as non-biological. Consequently, we set the fluorescence threshold to the highest fluorescence intensity value observed by the 99.5% approach (41,839 units; supplementary information, Figure S2b), applied it to all collected samples; henceforth named the 42k FL1-A threshold. The 42k threshold value aims to minimize any abiotic interference as it maximizes biological particles quantification. A fixed value has been chosen and applied to all samples given that having a different threshold value for each sampling event may result in quantification biases as bioaerosols with strong autofluorescence (e.g. pollen, fungal spores) can increase the threshold value and affect PBAP quantification in the population(s) within the threshold. The BD Accuri C6 flow cytometer used for the analysis of the samples maintains constant pre-optimized photomultiplier voltages and amplifier gain settings. As a result, the fluorescence intensity of particles is consistent from day-to-day, and the fluorescence intensity of a specific biological particle population having the same metabolic state and physiological characteristics must not show day-to-day variability (www.bdbiosciences.com). Under the 42k threshold approach PBAP concentrations in the population(s) within the threshold (e.g. LNA, Section 4.1) can be overestimated by up to a 0.5%. Furthermore, FCM experiments conducted with unprocessed Arizona Test Dust (ATD) show that the FL1_A intensity distribution of SYTO-13 stained ATD particles is very similar to unstained ATD particles, and 100% of the SYTO-13 stained ATD particles stay below the 42k threshold (supplemental information, Figure S14a and S14b), supporting the 42k threshold effectiveness to filter out abiotic particles.

Once the FL1-A threshold was determined, plots of FL1-A vs. SSC-A and FL1-A vs. FSC-A are used to define clusters of bioparticles with fluorescence that exceed the FL1-A threshold and a characteristic optical size (obtained from the FSC-A intensity) or particle internal complexity (obtained from the SSC-A

intensity). FL1-A vs. SSC-A plots were used to define the populations of bioparticles for PBAP quantification as clusters using SSC-A parameter were more defined and showed better spatial resolution than using FSC-A parameter. The limits of each population were also determined with Flow Jo (www.flowjo.com), using 2% contour plots (supplemental information; Figure S3) generated by equal probability contouring (i.e., 50 contour levels so that the same number of cells fall between each pair of contour lines). Populations above the FL1-A threshold value (41,839 FL1-A units) were considered biological (Section 4.1; e.g. HNA); the particles in the population within the threshold value (Section 4.1; e.g. LNA) having a FL1-A intensity greater than 41,839 units were counted as biological to determine the PBAP counts in the population. The total PBAP counts were considered as all particles counts having FL1-A fluorescence intensity above the determined threshold value minus the 15µm beads internal standard having FL1-A fluorescence intensity above the determined threshold value. The 15µm beads of known concentration and particle size allows for calibrating the optical size (supporting information, SI.7) of the bioparticles, as well as their concentration and departure from sphericity. The 15µm beads population showed fluorescence intensities comparable to the determined fluorescence threshold after been stained with SYTO-13 as it is known that molecular stains can be adsorbed on the surface of polystyrene beads (Eckenrode et al., 2005; Rödiger et al., 2011). The relatively high fluorescence intensity of the 15µm beads show populations within the threshold value (e.g. LNA, Section 4.1) cannot be rule out as being affected by unspecific staining of abiotic particles. However, populations above the threshold value (e.g. HNA, Section 4.1) should not be affected by such abiotic interferences.

3.2 WIBS data processing

15-minute average total aerosol and FBAP size distributions were obtained from the WIBS. FBAP was distinguished from the total aerosol using the Gabey et al. (2010) "trigger threshold" approach, which is applied as follows. First, the average "electronic fluorescence noise" and its standard deviation is determined for each channel (A, B, C) performing the Force Trigger (FT) calibration which consist to operate the WIBS without flowing air through the system. The FT calibration, carried out every 24hr, is critical for determining the lowest particle autofluorescence levels that robustly exceeds instrument electronic noise. FT calibrations measured the particle-free air background autofluorescence in the three WIBS channels (e.g. A, B, C), and measurements recorded the fluorescence intensity for 500 excitation flash events (Ziemba et al., 2016; Tropak and Schnaiter, 2013; Gabey et al., 2010). The threshold for each detector is then equal to the average fluorescence plus 2.5 times its standard deviation; particles with fluorescence intensities above this threshold value are classified as FBAP. Then, Perring et al. (2015) approach (Section 2.3) is applied to determine the combination of thresholds that provide the maximum concentration of PBAP and minimal interference from abiotic particles, which still remains an area of active research. It is important to note that the Gabey et al. (2010) threshold approach and the Perring et al. (2015)

FBAP types were applied to the WIBS-4A data and should not be directly compared to FBAP quantifications performed by the WIBS-3 in previous studies, owing to the channel A and B overlap on the latter. A detailed comparison between WIBS-3 and WIBS-4 models, as well as PBAP detection by both models, is further discussed in the supplemental information (SI.20).

In this study, thresholds for each channel were determined daily, and the total particle concentration, FBAP types (e.g. A, B, C, AB, BC, AC, ABC) concentrations and the total FBAP concentration (sum of the seven FBAP types) were used. From the data, 4h-averaged size distributions (using 15-minute average data) were generated for the total particles and all FBAP types in the 1-10µm range during the time SpinCon II run. Subsequently, WIBS overall sampling efficiency (aspiration efficiency + transport efficiency) was calculated using the Particle Losses Calculator (Von der Weiden et al., 2009) and applied to the 1-10µm size distributions for the sampling characteristics in our setup (15ft. sampling line with ¼ in. ID and 2.3 L min^{-1} flow rate; Figure S4a**)**. The sampling efficiency was calculated to be 67% for 5µm particles, with larger losses as size increased to 10µm. (supplemental information, FigureS4b). FCM and WIBS total particles and PBAP comparison was constrained to the 1 to 5µm range being the size overlap of both techniques. Also, the fractional composition of FBAP (based on number concentrations) was calculated to characterize its daily variability (Section 4.2), and compared against the daily variability of PBAP from the FCM analysis (Section 4.4).

4. Results and Discussion

4.1 FCM biopopulation identification and quantification

When the FCM results are plotted in terms of FL1-A fluorescence intensity versus SSC-A scattering intensity, four populations (Figure 2) emerge above the detection thresholds: low nucleic acid (LNA) particles, high nucleic acid (HNA) particles, pollen and the 15µm internal standard beads. EPM and SEM pictures (Supplementary Figures S5, S6, and S7) confirm the presence of these heterogeneous populations. SYTO-13 stains DNA and RNA, and the resulting single-cell FL1-A fluorescence intensity (Figure 2) is directly proportional to its nucleic acid content (Lebaron et al.,2001; Troussellier et al.,1999; Comas-Riu et al., 2002). Previously, SYTO-13 has effectively distinguish between HNA and LNA bacterioplankton and phytoplankton populations in fresh and seawater samples, and results are comparable to SYBR green II and SYBR green I, more specific DNA probes (Wang et al., 2010; Bouvier et al., 2007; Lebaron et al., 2001). However, corresponding populations in atmospheric PBAP have not been identified before. The SSC-A scattering intensity in Figure 2 changes as function of size, composition (e.g. cell refractive index) and complexity of the cell (e.g. internal structures or surface irregularities), and the strongest SSC-A intensity corresponding to the largest, most complex particles. Below we focus on each population to further understand the identified populations of biological particles.

The HNA size distributions are dominated by 3-5μm particles (mean diameter: 4.15 ± 0.06 μm; Supplemental Information, Figure S10) and the total concentration moderately correlated with RH. HNA were virtually non-existent during several extended dry periods (days with average RH < 70% during sampling, e.g. 4/9, 4/22 and 5/15) and well defined during periods of high humidity, especially after rain events (days with average RH > 70% and T > 18 °C during sampling episode; e.g. 4/7, 4/14, 4/15). Both of these characteristics suggest that HNA particles correspond to wet-ejected fungal spores (e.g., from the Ascospores and Basidiospores genus; Oliveira et al., 2009; Li and Kendrick, 1995). The LNA size distributions are dominated by 2-4 μm particles (mean diameter: 2.99 ± 0.06μm; Supplemental Information, Table S1) and dominated Atlanta PBAP composition during dry days. Many individual bacteria are likely in around 1μm, but the observed LNA particles are within the median aerodynamic diameter of culturable bacteria (~ 4μm) in continental sites (Despres et al., 2012). Bacteria in the atmosphere can be co-emitted together with larger particles (e.g. soil, plant fragments) and occasionally they are observed as clumps of bacteria cells (Burrows et al., 2009). In addition, several bacterial species observed in the atmosphere (Delort and Amato, 2018; Monier and Lindow, 2003; Baillie and Read, 2001) are within this sizes range (e.g., *Sphingomonas spp.:* 1.0 - 2.7μm; *Methylobacterium spp.:* 1- 8 μm, *Pseudomona syringae*: ~2.5μm, and *Bacillus anthracis*: 3-10μm), supporting LNA population may represent single or agglomerated bacterial cells. However, it is clear that heterogeneous populations will probably contain multiple types of microorganisms and that may be the case in the LNA population.

It is known that pollen may burst into tiny fragments when is suspended in water (e.g., Augustin et al., 2012; Taylor et al., 2007), potentially increasing the concentration of LNA particles and biasing concentrations. Although 0.2μm – 5μm pollen fragments can be generated upon rupture, pollen (e.g. Birch, Ryegrass, Oak, Olive) mainly breaks apart into submicron fragments by hydrolysis and favors fragmentation into small submicron (<1μm) particles (Taylor et al., 2007; Bacsi et al., 2006; Grote et al., 2003), not considered in our FCM analysis. An additional factor to consider in pollen fragmentation is the number of fragments generated per pollen grain. FCM applied to ragweed pollen suggests a 1:2 pollen-to-pollen fragments concentration ratio (Supplementary information, Table S2). Also, calculations based upon FCM-derived ragweed pollen and pollen fragments concentrations during this study (considering the total pollen mass added to the sample, 15μm mean diameter previously determined by Lin et al. (2013) and unit density) suggest approximately 67% of the ragweed pollen grains were intact after hydration and that each fragmented grain generates ~5 pollen fragments; in agreement with Bacsi et al. (2006), 35% of ragweed pollen fragments upon hydration. Overall, ragweed pollen results suggest FCM experiments do not have a considerable impact in pollen fragmentation and that pollen fragmentation will have a negligible effect on LNA concentrations. Ragweed pollen is one of the most abundant wind-driven pollen species in the United States and its emission peaks during fall, but can be also present during late spring and summer. It is

representative of the pollen species we see in the Atlanta area (Darrow et al., 2012) and results suggest pollen fragmentation would not generate a substantial amount of fragments. The low collection efficiency of SpinCon toward large particles (<14% for diameters above 5μm) and that pollen concentrations in our samples are generally two orders of magnitude lower than LNA concentrations (Figure S22; supplemental information) suggest a negligible effect of pollen fragments in LNA biological particle quantification. Pollen concentrations are 100-1000 times lower than bacteria concentrations in the atmosphere (Hoose et al.,2010). At least 100 supermicron (>1μm) pollen fragments will have to be released per pollen grain to considerably influence the LNA population, which has not been observed. Also, EPM results showed intact pollen and limited amounts of small debris among the particles identified in the atmospheric samples collected for this study. Particles with fluorescence intensities above the FL1-A threshold value in the LNA population were counted as biological, giving us the PBAP counts within the LNA population and will be referred henceforth as the "LNA-AT" population (Figure 2), where "AT" refers to above threshold.

The LNA population shows SYTO-13 fluorescence intensities that are about one order of magnitude lower than the HNA population, and the fluorescence intensity difference is consistent across all sampling events. Based on Bouvier et al.2007, cell populations with different metabolic activity (e.g. active and non-active), when detected by FCM, should observe a decrease in fluorescence intensity in consecutive sampling events if transition from the HNA to the LNA population, or vice-versa if transition from LNA to HNA population. The fluorescence intensity of the LNA and HNA populations show small variation throughout the sampling events (LNA-AT: $7.38 \times 10^4 \pm 1.39 \times 10^4$; HNA: $6.72 \times 10^5 \pm 2.30 \times 10^5$; Table S3) and no anticorrelation is observed in the studied parameters (FSC-A, SSC-A, FL1-A), which supports we have in fact two distinctive population of bioaerosols (Supplemental Information; Figures S23 and S15).

A population of strongly fluorescing and very large particles (10-20μm, avg. average geometric mean diameter 12.3 ± 1.7μm) was identified (Figure 2). This population also strongly autofluoresces in the FCM when SYTO-13 was not added to the sample (SI.7, Figure S11). All together this indicates a population of pollen particles, as they are known to contain cell wall compounds (i.e., phenolic compounds, carotenoid pigments, Phenylcoumarin) that fluoresce more strongly than the proteins and cytosolic compounds responsible for bacteria/fungi autofluorescence (Pöhlker et al., 2012; Hill et al., 2009; Pöhlker et al., 2013). The pollen population was not well-defined during all sampling events; whenever present, pollen was characterized by concentrations ($\sim 10^2\ m^{-3}$) consistent with reported values (Despres et al., 2012), which are also much lower than LNA-AT and HNA concentrations. As a result, pollen population was systematically gated using a perfect square between 10^6 and 10^8 intensity units in the FL1-A vs. SSC-A plot for each atmospheric sample. LNA-AT, HNA and pollen counts, acquired by the 42k threshold approach were used to calculate liquid-based (mL^{-1} of sample solution) and air-based (m^{-3} of air) concentrations for each

503 bioaerosol population as detailed in the Supplemental Information. The total PBAP concentration on each
504 sample consisted of all non-bead particles above the 42k fluorescence threshold given that a non-negligible
505 biological particle concentration was not constrained in the gated populations. Even though the 2% contour
506 plots effectively allowed population gating, 16.5 ± 7.3% of the total PBAP are not attributed the identified
507 populations. The biological particles not constrained by FlowJo 2% gating, henceforth named as the
508 "unclassified" bioparticles, showed the highest concentrations when both HNA and LNA populations are
509 densely populated (4/16, 4/28 and 5/14; Figure 5). The lowest concentrations were observed when just the
510 LNA population is identified (4/9, 4/22, 5/15; Figure 5) and when the LNA and HNA populations are
511 identified after the rain event on 4/14. The observed behavior shows that the unclassified bioparticle
512 concentrations is linked to the heterogeneity of the biological populations and the concentration of the gated
513 populations (e.g. HNA, LNA and Pollen). The "unclassified" bioparticles concentration ranges from 8.1 x
514 10^2 m^{-3} to 1.3 x 10^4 m^{-3} (avg. 4.2 x 10^3 ± 3.3 x 10^3) and they are not constrained to a specific size range.
515 Most of the unclassified bioparticles are far from the centroids of the gated populations. They can indeed
516 be formed by fragmentation or accretion, or also be related to plant debris (i.e., irregular bioparticles) that
517 are characterized by a very broad size, internal complexity and nucleic acid content distributions. In
518 addition, we must note that additional concentration corrections are required owing to the sampling
519 efficiency of the SpinCon II, but will be considered in sections 4.3 and 4.4.

520 Before SpinCon II sampling efficiency corrections are applied, FCM total particle concentrations range
521 from 2.6 × 10^4 m^{-3} to 2.9 × 10^5 m^{-3}, with increasing concentrations toward the end of the sampling period.
522 In addition, total PBAP concentration averaged 2.4 × 10^4 ± 1.1 x 10^4 m^{-3} (coefficient of variation, CV, 13%;
523 defined as the standard deviation over a triplicate FCM measurements over the average concentration).
524 LNA-AT ranged between 6.8×10^2 and 2.9 ×10^4 m^{-3} (average: 1.1×10^4 m^{-3}; CV: 20%), HNA(fungal spores)
525 between 4.7×10^3 and 1.9×10^4 m^{-3} (average: 1.1×10^4 m^{-3} ; CV: 15%) when above the detection limit (n=12),
526 and pollen from 1.3×10^2 to 1.2×10^3 m^{-3} (average: 3.6×10^2 m^{-3}; CV: 21%). These concentration levels are
527 consistent with microscopy-based studies in urban environments for bacteria (e.g., 1.7×10^4 ± 1.3×10^4 m^{-3}
528 in springtime Birmingham, UK; (Harrison et al., 2005); fungal spores (1.8×10^4 ± 1.1×10^4 m^{-3} in Vienna,
529 Austria between April-June; Bauer et al., 2008); and pollen (between 5.69×10^2 m^{-3} to 6.144×10^3 m^{-3} in
530 Medellin, Colombia; Guarín et al., 2015). Also, additional experiments performed in September 2015,
531 described in Figure S7 of the supplemental information (supplemental information, SI.6), showed that EPM
532 and FCM-based quantifications agree within an order of magnitude. This is consistent with Lange et al.
533 (1997), whom also found that FCM gives higher quantifications than EPM microscopy when studying *P.*
534 *aeruginosa* pure cultures and airborne bacteria collected from a swine confinement building in Iowa, USA.

To better understand SYTO-13 fluorescence intensity differences between the identified (e.g. LNA-AT, HNA and pollen) populations in the atmospheric samples and their metabolic/stress state, FCM experiments were conducted with air-isolated bacteria (F8 strain; De Leon Rodriguez, 2015), ragweed pollen and yeast (*S. cerevisiae*; Y55 strain) mixtures to compare the SYTO-13 fluorescence intensity and the scattering properties of the pure cultures to those seen in the atmospheric samples. Pure culture experiments aimed to: (1) serve as positive controls to ensure SYTO-13 effectively stains bacteria, fungi and pollen, and (2) acquire reference fluorescence and scattering properties on each pure culture population. Pure cultures and atmospheric samples are summarized in Tables S3, S4 (supplementary information; FCM pure culture experiments) respectively. The LNA-AT population showed SYTO-13 fluorescence intensity up two orders of magnitude lower than F8 bacteria. The HNA population showed an order of magnitude lower SYTO-13 fluorescence intensity than Y55 HNA yeast, and, within the same magnitude for the LNA Y55 yeast. The HNA and LNA yeast populations in the pure culture experiments (Figure S13a) have one order of magnitude difference in FL1-A fluorescence intensity and may represent yeast populations with different metabolic states. Atmospheric and ragweed pollen populations had similar SYTO-13 fluorescence intensities and Figure S13c shows pollen fluorescence intensity may go up to 10^8. The lower SYTO-13 fluorescence intensity of the atmospheric populations may be related to genetic material degradation from exposure to atmospheric stressors; depending on the physiological characteristics of each population (Zhen et al., 2013; Amato et al., 2015). Our results also agree with Guindulian et al. (1997), showing that *E.coli* overnight cultures have higher SYTO-13 fluorescence intensity than starved *E.coli* population. Overall, FCM pure culture results suggest microbes starve in the atmosphere, leading to a possible reduction or leakage of the amount genetic material enclosed within each cell. Sampling can also stress cells, even disrupt the wall/membrane of the cell and lead to genetic material leakage (Zhen et al., 2013).

Pollen, HNA and LNA-AT atmospheric populations showed different SYTO-13 fluorescence intensities. Pollen showed the highest fluorescence intensity**,** followed by the HNA and LNA-AT (fraction of LNA above threshold; Figure 2) populations, respectively (Figure 2; Table S4). Guindulian et al. (1997) FCM results with starved bacterioplankton from seawater samples treated with DNase/RNase showed SYTO-13 fluorescence intensity can be related to the DNA content of starved bacterioplankton due to the low amount of RNA enclosed in starved cells. Taking in consideration our results and previous studies, we can suggest that Pollen, LNA-AT and HNA populations in the atmospheric samples are differenced by their DNA content, which can in part explain SYTO-13 fluorescence intensity difference between them. We also acknowledge DNA sequestration by bacteria, fungal spores and pollen may differ and their cell membrane characteristics will ultimately determine how much stress the cells will sustain before they completely rupture. SYTO-13 is a highly permeable stain and effectively detects nucleic acids (DNA and RNA) of bacteria endospores and vegetative cells (Comas Riu et al.,2002). Fungal spores have also been effectively

stained by DNA/RNA probes (Bochdansky et al., 2017; Chen and Li et al., 2005), but some fungal spores might not be equally stained due to their harder cell wall, and chromatin-binding of DNA (Standaert-Vitse et al., 2015). Future work is needs to further study this.

4.2 WIBS total concentration and FBAP daily variability

WIBS-4A collected data continuously throughout the period; for comparison against the SpinCon II 4h liquid batch samples, WIBS data was averaged to the SpinCon II sampling times (Table 1). WIBS total particle concentration (1-5µm diameter) ranged from 2.0×10^5 to 1.0×10^6 m^{-3} in agreement with observed particle concentrations in previously studied urban environments during Spring/Summer months like Helsinki, Finland (UV-APS avg. 1.6×10^5 m^{-3}; Saari et al., 2014) and Karlsruhe, Germany (WIBS-4 avg. 6.9×10^5 m^{-3}; Tropak and Schnaiter et al., 2013). 4h average total particles concentrations in Figure 3a show particle concentrations declined during rain episodes (during or post-rain: e.g. 4/15, 4/16, 4/28, 4/29, 4/30) as wet removal of PBAP is most efficient. However, during dry (no rain) episodes total particle concentrations built up in the atmosphere. To better understand the day-to-day variability of different FBAP types, the seven Perring et al. (2015) FBAP categories (e.g. Type A, B, C, AB, AC, BC and ABC) were studied plus the NON-FBAP type constituting particles that do not fluoresce in any channel (e.g. channel A, B, C). NON-FBAP concentrations are one order of magnitude higher than FBAP concentrations, and NON-FBAP, hence traced WIBS total particles throughout all sampling events (Figure 3a). Total FBAP concentrations also show similar behavior to the total particle concentration (Figure 3a) and it suggests non-biological particles can be biasing the total FBAP concentration. The variability of the total FBAP concentration is mainly linked to type A and type B concentrations as overall they constitute the two largest fractions to the total FBAP concentration (Figure 3b), and both FBAP types have previously misidentified non-biological particles as FBAP (Tropak and Schnaiter et al., 2013; Yu et al., 2016). As a result, our study considers the total FBAP concentration as the upper limit, and ABC type concentration as the lower limit of FBAP concentration in Metro, Atlanta. Type B dominates the FBAP fractional composition (Figure 3b), which has been linked to possible non-biological interferences from black carbon (Yu et al., 2016) and polycyclic aromatic hydrocarbons (PAHs) emitted from combustion sources. Total FBAP fraction ranges from 16% and 43%, and ABC fraction ranges from 1.3% and 9.2% of the total particles in the 1 to 5µm size range. ABC type fractions and ABC type concentrations are within the values observed by Tropak and Schnaiter (2013) using WIBS-4 in Karlsruhe, Germany; averaging 2.9×10^4 m^{-3} (when considering the sum of AC and ABC types) and constituting 7% of total coarse mode particles (0.8µm-16µm).

ABC type concentrations show an interesting variability throughout the 15 sampling events, as ABC reaches its maximum concentration on 4/14, on a warm and humid day after a rain event, concurrently

when the FCM HNA population also reaches its highest concentration – strongly suggesting ABC particles are fungal spores. (Figure 3a, Table 1). Furthermore, WIBS high resolution data in Figure S24 shows the enhancement of AB and ABC type right after the beginning of the rain event on 4/13 (6pm; night before sampling on 4/14) and is not correlated to NON-FBAP concentrations; FBAP concentration enhancement previously linked to wet-ejected fungal spores (Huffman et al., 2013; Gosselin et al., 2016). Gosselin et al. (2016) used WIBS-3 in the Rocky Mountains, Colorado showing ABC type fractional composition enhances after rain events to dominate the total FBAP composition and the enhancement is correlated to mannitol and arabitol concentrations (fungal spore tracers), which have been previously linked to Ascomycota and Basidiomycota spores emitted by the wet-ejection mechanism (Elbert et al., 2007). In addition, ABC type constitute a considerable fraction (~20%) of total FBAP during dry days in the Rocky Mountains possible because such highly vegetative environments maintain a high background of fungal spores (Huffman et al., 2013). However, urban environments like Metro Atlanta are not necessary dominated by fungal spores and its FBAP composition will be affected by the biological sources close to city (e.g. forests), local emissions and meteorology. The overall FBAP composition in metro Atlanta (Figure 3b) is dominated by type B (avg. fraction: 33 ± 9%), type A (avg. fraction: 22 ± 5%) and type AB (avg. fraction: 22 ± 5%) particles. Type ABC constitute 12 ± 6% of the total FBAP and it reaches 30% on 4/14, comparable to values observed by Gosselin et al., 2016 in the Rocky Mountains. The dominance of type B particles has been observed in the polluted atmosphere of Nanjing, China using WIBS-4A were type B constituted ~ 45% of the total PBAP and type B (~ 2×10^6 m^{-3}) concentrations were up to two orders of magnitude higher than type A concentrations (~5×10^4 m^{-3}) suggesting a high likelihood of interference from abiotic particle sources. However, Metro-Atlanta shows much lower total particle concentrations than Nanjing, China (~10^7 m^{-3}) and type A and type B concentrations are within the same order of magnitude. Furthermore, Perring et al. (2015) have shown type B particles constitute a considerable fraction of the total supermicron particles across the United States, being ~15% and ~25% over (altitude >100m) the Southeastern US and Southwestern US, respectively. Total particle and NON-FBAP size distributions in Figure 3c peaked at ~1µm. Similarly, types A, B, AB size distributions (Figure 3d) peaked close to 1µm showing that interferences by non-biological particles cannot be rule out. However, ABC type size distribution (light blue line, Figure 3d) is dominated by 3-5µm particles and ABC type particles may have come from a different source to other FBAP types as they get enhanced after rain events (e.g. 4/14; Table 1). Yu et al. (2016) also observed 4-6µm ABC type particles in the highly polluted Nanjing, China, but ABC type bimodal size distributions showed a peak between 1-2µm and a second peak between 4-6µm. In addition, ABC type number fractions in Nanjing, China correlated to black carbon mass fractions suggesting a considerable influence by combustion related particles and no rain events occurred during the sampling period. The difference between Metro Atlanta and Nanjing, China ABC type size distributions

suggest ABC type is not influenced by combustion related particles in Metro Atlanta. Overall, results show FBAP concentration (1-5µm) ranges from 10^4 -10^5 m^{-3} in metro Atlanta and wet-ejected fungal spores concentration, detected by ABC type, can constitute up to 30% of the FBAP (1-5 µm) after rain events.

4.3 Correlation of HNA population with ABC type

A quantitative comparison between WIBS-4A total particle and FCM total particle concentrations was subsequently performed and we focused the analysis to the 1 to 5µm size range as SpinCon sampling efficiency is reduced significantly above 5µm (≤14%; Kesavan et al., 2015). WIBS-4A and FCM total particle concentrations differed by about one order of magnitude (for optical diameter, d_o, greater than 1.5µm) and particle concentration difference increased for particles with $d_o < 1.5$ µm as shown in the size distribution (geometrically averaged across the 15 SpinCon II sampling events) in Figure 4a. The largest difference between WIBS-4A and uncorrected FCM size distributions seems to be related to SpinCon II having a cutoff size close to 1µm, reducing significantly its sampling efficiency. Even with the observed difference in the magnitude of the concentrations between the two techniques, ABC type and HNA concentrations traced throughout all the sampling events and are moderately correlated ($R^2 = 0.40$, P-value = 0.016; Figure 4b) and showed similar size distributions in the 1 to 5µm range as shown in Figure S12a. HNA and ABC type were both dominated by 3-5µm particles and its seems both are detecting the same type of biological particles. In addition, AB type showed a weak correlation with HNA concentrations (R^2 = 0.17), but their size distributions differed as type AB peaks close to ~1µm (Figure 3d). ABC is the only FBAP type showing a considerable correlation to the HNA population, and LNA-AT population is not correlated with any FBAP type. Overall, ABC type and HNA correlation is an important step forward to better understand the effectiveness of WIBS-4A FBAP categories to provide speciated PBAP concentrations in urban areas. ABC type particles have shown substantial concentrations (10^4 -10^5 m^{-3}; Perring et al., 2015; Ziemba et al., 2016) across the US. The highest ABC fraction of the total FBAP was observed in Panhandle, Florida during an airborne study among multiple environments studied using WIBS-4A to sample from the California coast to central Florida, suggesting ABC type particles are ubiquitous in the US (Perring et al., 2015). Previous studies (Healy et al., 2014, Huffman et al., 2013) have shown correlations between LIF technology (e.g. WIBS-4 and UV-APS) fluorescence channels and fungal spores number concentrations, especially during fungal spores invigoration after rain events. Healy et al. (2014) used WIBS-4 in Killarney National Park, Ireland (e.g. high vegetative rural area) finding correlations between channel B (FL2; $R^2 = 0.29$) and channel C (FL3; $R^2 = 0.38$) concentrations and fungal spores concentrations (collected by Sporewatch impactor and quantified by microscopy). Gosselin et al. (2016) observed stronger correlations between fungal spores (inferred from mannitol and arabitol concentrations) and WIBS-4 concentrations in the Rocky Mountains, but our study in Atlanta, GA was carried out in completely different environment (e.g. highly-populated urban environment). Now for the first time FCM

669 HNA population have shown a correlation with WIBS-4A ABC type and suggests ABC type category
670 detects wet actively ejected fungal spores in Metro Atlanta (e.g. urban area). In addition, recent WIBS-4A
671 experiments using pure cultures have shown ABC type detects well several fungal spores (e.g. *Aspergillus*
672 *Versicolor* & *Botrytis spp*.) and small pollen grains, but detection may vary across instruments (Hernandez
673 et al., 2016).
674 FCM concentrations were corrected based on correction factors (CF) calculated upon the
675 comparison of ABC and HNA size distributions (1 to 5µm) for each sampling event given (1) ABC type
676 and HNA population similar size distributions and number concentrations (1 to 5µm) correlation, and, (2)
677 WIBS-4A provides us representative concentrations of airborne particle concentrations in Metro Atlanta
678 after sampling losses being corrected (Section 3.2). Concentration correction factors were determined for
679 each sampling episode by taking the quotient of ABC type to HNA concentrations over the 1-5µm size
680 range. The resulting size-dependent correction factor (Figure S12b) was then applied to the FCM size
681 distributions, giving the "corrected FCM" bioaerosol data (between 1 and 5 µm). Figure 4a shows that the
682 corrected FCM total particle average size distribution traces WIBS-4A size distribution, allowing us to
683 correct for SpinCon II low collection efficiency and to better constrain the magnitude of FCM
684 concentrations. Our approach to calculate the estimated collection efficiency (ECE) considers all the
685 processes that affect the concentration of PBAP, from collection to final quantification in the FCM. Figure
686 S12b compares Kesavan et al. (2015) collection efficiencies determined for SpinCon I and the estimated
687 collection efficiency calculated upon the CF calculation (ECE = 1/CF) and shows the ECE of the SpinCon
688 II is lower that Kesavan et al. (2015) below 3µm and performs better for particles above 3µm, but above
689 3µm Kesavan et al (2015) collection efficiency is within the uncertainty of our calculations. Our lower ECE
690 values (Figure S12b) for particles below 3µm can be related to SpinCon sampling time as Kesavan et al.
691 (2015) experiment were conducted in a short period of time (e.g. 10-15 min) and ours took place for 4 h
692 The main mechanisms leading to below 3µm particle losses could be their re-aerosolization over time being
693 lost through the blower exhaust of the SpinCon II (Figure 1). Also, coagulation of small particles over time
694 can not be rule out, but future work is needs to study it. Although SpinCon/FCM results correction based
695 on the HNA and ABC type size distributions comparison effectively constrain the efficiency of the
696 SpinCon/FCM analysis in this study, corrections are limited to the 1 to 5µm size range and must
697 acknowledge that the specific sampling may stress cells and affect their detection.
698

699 **4.4 PBAP populations after collection/detection corrections**

700 After correction through the application of the ABC correction factors, FCM total particle
701 concentrations (1 to 5µm avg.: $5.5\times10^5 \pm 5.1\times10^5$ m^{-3}; Figure 5a) are within the same order of magnitude

as WIBS-4A concentrations (1 to 5µm avg.: $5.4\times10^5 \pm 2.9\times10^5$ m^{-3}; Figure 3a), and continue to exhibit substantial variability. The HNA (e.g. fungal spores) population showed a substantial invigoration during three sampling events (4/7, 4/14, 4/15; Figure 5a and 5b). To better understand the role of meteorology on PBAP composition, 24 hr-averaged temperature and relative humidity were used to express the prevailing temperature and relative humidity (RH) during each sampling event, considering the residence time of microorganisms (e.g. bacteria and fungal spores) before sampling. Sampling events were classified into four regimes based on the average diurnal (24hr avg.) relative humidity and ambient temperature, with T= 18 °C (65 °F) to differentiate between warm and cold days, and, RH = 70% to differentiate between humid and dry days. During the 15 sampling days, temperature ranged from 10.4°C to 31.2°C, and RH varied from 19.0% to 97.0% in Atlanta, GA (Look Table S4; supplemental information) The temperature and RH threshold values were chosen based on the observations and understanding that a combination of temperature and RH within these threshold values can significantly impact bioaerosol composition. For instance, humid and warm conditions may lead to the invigoration of fungal spores by wet ejection from plants (Ingold, 1971), on contrary, PBAP will get stressed when exposed to warm and dry conditions. The sampling times, RH, ambient temperature and meteorological categories of each SpinCon II sample is presented in Table 1.

Humid and warm days (4/7, 4/14 and 4/15; light green shaded areas in Figure 5a) were characterized by well-defined HNA and LNA-AT populations. These sampling episodes had the highest average HNA (fungal spore) concentration ($4.0\times 10^4 \pm 1.3\times10^4$ m^{-3}) among the four meteorological regimes and during these sampling events HNA constituted ≥ 77 % of the total PBAP. Among the humid and warm days (Figure 5a and 5b), average LNA-AT, HNA and "unclassified" bioaerosol compositions were 6.1%, 84.0% and 9.9%, respectively of the total PBAP number. Also, the humid and warm days occurred after rain events, which can be linked directly to the strong fungal spore invigoration (Huffman et al., 2013). Before sampling, early morning precipitation occurred during 4/14 and 4/15, as well as during the night of 4/6. Precipitation did not occur during sampling in any of the humid and warm days. The FCM results (Figure S15a-c) that display the PBAP population between 4/7 and 4/9 show a disappearance of the (HNA) fungal spore population during the transition from a "humid and warm" day (4/7) to a "dry and warm" day (4/9). Figure 5b shows how the HNA contribution to the total PBAP goes down on 4/8 when RH decreases and is undetected on 4/9. Furthermore, Figure 6a-c shows FL1 vs. SSC-A plots for 4/14 to 4/16 consecutive sampling periods, where a marked increase in the LNA-AT concentration from 4/15 to 4/16 goes together with a striking decrease in the HNA concentration. HNA fraction went down from 92.0% to 34.1% of the total PBAP and LNA-AT concentration went up from 3.8×10^3 m^{-3} to 2.9×10^4 m^{-3}. Humid and Warm days had the lowest averaged PBAP concentration ($4.6 \times 10^4 \pm 9.8 \times 10^3$ m^{-3} in the 1 to 5µm range) among the

four meteorological regimes, a possible effect of the bioaerosols being lost by wet scavenging, resulting in the enhancement of fungal spore contribution to the total PBAP number concentrations. The unclassified biological particles concentration also showed its lowest contribution (2.9×10^3 m^{-3}; 9.9%) to the total PBAP number concentration during these events, when the HNA and LNA populations are best identified by the 2% contour plots.

Cold and humid days (4/16 and 4/29; light yellow shaded areas in Figure 5a) also showed well-defined HNA population, and HNA contributed on average to 29.5 ± 6.5 % of the total PBAP concentration (1 to 5μm). On 4/16 drizzling took place by the end of the sampling period, but no accumulated rainfall was measured by the meteorological station. However, on 4/29, accumulated rainfall averaged 0.04in. from 11:55 AM to 2:20 PM (Figure S21). The similar HNA concentration between "Humid and Warm" and "Humid and Cold" days seen in Figure 5a and the lower contribution of HNA to the total PBAP during the "Humid and Cold" days may be linked to previously suggested bacteria emissions by droplet soil impaction during rain events (Joung et al., 2017). Bacteria emission by soil impaction can increases airborne LNA-AT concentration and HNA (fungal spores) will have a lower contribution to the total PBAP even when the fungal spore concentration is high during rain events. Both cold and humid days showed a considerable difference in LNA-AT contributions to the total PBAP concentration. On 4/16 and 4/29 LNA-AT constituted 45.2% and 65.3% of the total PBAP concentration, respectively (Figure 5b). The difference in the LNA-AT contribution to the total PBAP can be linked to the intensity of precipitation, as it shapes the composition (e.g. size and types) of microbes suspended in the atmosphere during the different stages of a rainfall (e.g. before, on set, during and after a rainfall; Yue et al., 2016).

Six of the fifteen sampling days were classified as warm and dry (4/8, 4/9, 4/22, 5/13, 5/14, 5/15; light orange shaded areas in Figure 5a) and it did not rain before or during any of these days (Table 1). During warm and dry days, HNA had the lowest averaged concentration ($8.7\times10^3 \pm 1.2\times10^4$ m^{-3}) among the four meteorological categories. In addition, during three dry and warm days (4/9, 4/22 and 5/15) the HNA population was undetected. This behavior can be related to the fact that high RH drives fungal spore emissions by wet ejection, but soil wetness could also affect emissions because the HNA population was detected in other warm and dry days with comparable RH (Huffman et al., 2013; Gosselin et al., 2016). The air mass trajectories reaching Atlanta during each sampling event could also affect the biological particles composition. For example, on 4/22, when the HNA was undetected, the 500m and 100m 72 h backward air mass trajectories reaching Atlanta came from the NW (US/Canada border) at high altitudes and do not spend more than 24h near surface. This air mass could affect bioaerosol composition with minimal influence from local bioaerosol emissions. However, the enhancement or the depletion of the HNA population have not been linked to specific air masses trajectories. Overall, warm and dry days prevail

768 during springtime in Atlanta and LNA-AT contribution (avg.: $3.4\times10^4 \pm 2.5 \times10^4$ m^{-3}) may represent the
769 bioaerosol background of Atlanta.

770 Four of the fifteen sampling days (4/21, 4/23, 4/28 and 4/30; light blue shaded areas in Figure 5a) were
771 characterized by cold and dry conditions (Table 1). PBAP were dominated by LNA-AT during these events,
772 as can see in Figure 7a-c, where LNA population are the dominant contributors to PBAP number. HNA
773 population was diminished in Figure 7a (4/21) & Figure 7c (4/23) during cold and dry days and disappeared
774 in Figure 7b during a warm and dry day. Overall, HNA was detected during cold and dry days, but showed
775 lower contributions to the total PBAP number concentration than humid days. Among cold and dry days,
776 the PBAP population (1 to 5 μm) was composed on average of 72.6 ± 10.1% LNA-AT and 16.5 ± 8.2%
777 HNA. Cold and dry days had on average the highest LNA-AT ($5.3\times10^4 \pm 1.8\times10^4$ m^{-3}) and total PBAP
778 ($7.3\times10^4 \pm 2.0\times10^4$ m^{-3}) number concentrations (1 to 5μm) among the four meteorological categories,
779 reaching the PBAP maximum concentration on 4/23 (Figure 5a).

780

781 **4.5 PBAP day-to-day variability in Metro Atlanta: FCM vs. WIBS**

782 Although WIBS and FCM possess different methodologies, they show similar trends providing a
783 good understanding of the daily variability of PBAP in Metro Atlanta. FCM PBAP fraction (1 to 5μm)
784 ranges from 3.8% to 69.2% of the total particles and the highest PBAP fraction (69.2%) and HNA
785 concentration is observed on 4/14 ($5.25\times10^4 \pm 5.89\times10^3$ m^{-3}). The total FBAP fraction (1 to 5μm) ranges
786 from 16% to 43%, but it reaches its maximum on 4/15. However, ABC fraction of the total WIBS particle
787 concentration ranges from 1.3% to 9.2% and it reaches its maximum on 4/14. Even when the magnitudes
788 of the PBAP and FBAP fractions differ on average by a factor of ~ 2 throughout the sampling period, both
789 techniques agree an enhancement in the total biological particles takes place between 4/14 to 4/16. Given
790 the uncertainty of the two methodologies, it is remarkable that there is such agreement between WIBS and
791 FCM results.

792 Among the four meteorological categories, humid and warm days characterize for showing the
793 highest HNA, A type, AB type and ABC type concentrations suggesting that A and AB types may also be
794 related to wet-ejected fungal spores in Metro Atlanta; this possibly explains why the ABC fraction of the
795 total FBAP in 4/7 is not as high as on 4/14 and 4/15 (Figure 3b), and differs with the behavior observed by
796 the HNA population on 4/7. The LNA-AT population does not show a correlation to any specific FBAP
797 type and shows it highest concentrations during dry and cold days. In addition, LNA-AT concentrations are
798 anticorrelated with type B concentrations (Figure S19, correlation coefficient, r = -0.59; R^2 =0.30) during
799 dry (both cold and warm) days, when LNA-AT dominates the total PBAP concentration. Given that type B
800 particles have been previously correlated to abiotic particles (e.g. black carbon) in urban environments (Yue

et al., 2017), LNA-AT and type B anticorrelation suggests that LNA-AT particles may in fact represent a heterogeneous bioaerosol population. That LNA-AT is not correlated with any FBAP type gives rise to two possibilities: (1) if LNA-AT population is mainly composed of bacteria or agglomerated bacteria, then it is possible that they are detected by multiple FBAP types and is not attributed specifically to one of them; (2) the intrinsic fluorescence of LNA-AT particles is too low and a high fraction of them is abiotic. It is challenging to determine what PBAP types each WIBS FBAP type is mainly detecting. Based on WIBS-4A results in Metro Atlanta, ABC type detects wet-ejected fungal spores, but still unclear what PBAP types are detect by the other FBAP types or if they just capture a high fraction of non-biological particles. FBAP types and WIBS total particles correlations in Figure S17 show all FBAP types are correlated to WIBS total particles, but ABC and AB types show the lowest correlations (type AB: R^2 =0.101; type ABC: R^2 = 0.1266).

Figure 8 shows FCM total PBAP (black line), ABC type (light green), FL1(Channel A; dark green line) and total FBAP (blue line) concentrations, where the FL1 concentration ([FL1]) constitutes the sum of the number concentrations of types A, AB, AC, and ABC ([FL1] = [A] + [AB] + [AC] + [ABC]; Gabey et al., 2011; Healy et al., 2014). Throughout the April-May 2015 sampling events, total PBAP concentrations (1 to 5µm) were mainly constrained between the FL1 and ABC type concentrations suggesting FL1 and ABC type represent the upper and lower bound PBAP concentrations in Metro Atlanta, respectively. It also important to highlight that FCM PBAP concentrations are closer to the ABC type concentrations before April 16 when the HNA population dominates, but then after April 16 FCM PBAP concentrations are closer to FL1 concentrations when LNA-AT starts to dominate the total PBAP concentration. In addition, Figure 8 shows that total FBAP (sum of type A, B, C, AB, AC, ABC) exceeds the (corrected) PBAP concentrations in Metro Atlanta.

5. Conclusions

In this study we presented the development and testing of an effective FCM protocol to identify and quantify bioaerosol populations. The FCM protocol, designed to constrain any particle accumulation due to cleaning or by fluid supplies, successfully quantified the day-to-day variability of bioaerosols in the Atlanta Metro area. It is the first FCM study to detect well-defined LNA (low nucleic acid) and HNA (high nucleic acid) atmospheric biological populations under different meteorological scenarios. FCM results show dynamic bioaerosol populations in Atlanta leading to a 84.0% of HNA (wet-ejected fungal spores) and 6.1% LNA-AT contribution to the PBAP number (1 to 5µm range), respectively, during humid and warm days after rain events. However, LNA-AT dominates warm and cold dry days, constituting 72% of the PBAP number concentration.

WIBS-4A and SpinCon II collocated sampling showed that the HNA and ABC type concentrations are well correlated (R^2=0.40) and display similar size distributions. We therefore conclude that both instruments detect the same particles, and used empirical collection/detection efficiency factors to correct the FCM size distributions and concentrations in the 1 to 5µm diameter range. WIBS-4A and FCM results suggest Metro Atlanta PBAP concentrations range between 10^4 - 10^5 m^{-3} (1 to 5µm) and they can constitute a substantial fraction of coarse mode particle concentration (WIBS-4A: 43%; FCM: 69%), comparable to the PBAP coarse mode fraction in highly vegetated environments. The FCM LNA-AT population, possibly containing bacterial cells, did not correlate to any FBAP type. The fact that the LNA-AT population is not correlated with a specific FBAP type suggests it may be particularly challenging to use LIF techniques to distinguish bioaerosols with low intrinsic autofluorescence from non-biological particles, especially given the heterogeneities introduced by the large biodiversity of airborne microbes. The possible influence of abiotic particles in the LNA-AT population can also explain the lack of correlation between LNA-AT and FBAP types given that the FCM threshold approach does not ensure total exclusion of abiotic particles. In addition, the unspecific binding of SYTO-13 to abiotic particles cannot be ruled out in the LNA-AT population. FCM comparison between atmospheric and pure culture samples showed lower SYTO-13 fluorescence intensities in the atmospheric samples and suggests a degradation in the genetic material of PBAP, possibly caused by the limited nutrients and strong stress prevailing in the atmosphere, which further challenge the ability of LIF to distinguish LNA-AT.

In summary, this study has shown for the first time that FCM can effectively identify, quantify and study the daily variability of heterogeneous PBAP populations (e.g. HNA, LNA-AT and pollen) with different genetic material content in atmospheric samples. We also show that a number of FCM and WIBS-4A populations are largely correlated and therefore can be used to identify the nature of the FBAP detected in the latter. Our results finally show that the detection and quantification of bacterial cells in atmospheric samples remains a challenging task and is best achieved through the combination of techniques.

Acknowledgments

We acknowledge support from a Georgia Power Faculty Scholar chair, a Cullen-Peck Faculty Fellowship, a Dreyfus Foundation Postdoctoral Fellowship in Environmental Chemistry, NASA, a NASA Earth System Science Fellowship (grant no. 80NSSC17K0434). We also acknowledge support from project PyroTRACH (ERC-2016-COG) funded from H2020-EU.1.1. - Excellent Science - European Research Council (ERC), project ID 726165. We also thank Prof. Rodney Weber for helpful suggestions on the SpinCon II flow calibration.

Competing interests

The authors declare no competing interests.

Author contributions

AN, AN, KK and MB conceived the study. AN, NDLR, SW developed the modified biosampler. AN and NDLR developed the FCM analysis and sampling protocol. AN, NDLR carried out measurements, and SW helped support with analysis of the biological samples. LZ, BA provided the WIBS and helped with its setup and initial data analysis procedure. AN, AN worked on the analysis, write codes to interpret the data and developed the analysis protocol to combine the FCM and WIBS analysis outlined here. AN and AN wrote the paper, and all authors contributed with comments and modified text.

References

Amato, P., Joly, M., Schaupp, C., Attard, E., Möhler, O., Morris, C. E., Brunet, Y., and Delort, A. M.: Survival and ice nucleation activity of bacteria as aerosols in a cloud simulation chamber, Atmospheric Chemistry and Physics Discussions, 15, 4055-4082, 10.5194/acpd-15-4055-2015, 2015.

Augustin, S., Hartmann, S., Pummer, B., Grothe, H., Niedermeier, D., Clauss, T., Voigtländer, J., Tomsche, L., Wex, H., and Stratmann, F.: Immersion freezing of birch pollen washing water, Atmospheric Chemistry and Physics Discussions, 12, 32911-32943, 10.5194/acpd-12-32911-2012, 2012.

Bacsi, A., Choudhury, B. K., Dharajiya, N., Sur, S., and Boldogh, I.: Subpollen particles: carriers of allergenic proteins and oxidases, J Allergy Clin Immunol, 118, 844-850, 10.1016/j.jaci.2006.07.006, 2006.

Baillie, L., and Read, T. D.: Bacillus anthracis, a bug with attitude!, Current Opinion in Microbiology, 4, 78-81, https://doi.org/10.1016/S1369-5274(00)00168-5, 2001.

Bauer, H., Claeys, M., Vermeylen, R., Schueller, E., Weinke, G., Berger, A., and Puxbaum, H.: Arabitol and mannitol as tracers for the quantification of airborne fungal spores, Atmospheric Environment, 42, 588-593, 10.1016/j.atmosenv.2007.10.013, 2008.

Bauer, H., Schueller, E., Weinke, G., Berger, A., Hitzenberger, R., Marr, I. L., and Puxbaum, H.: Significant contributions of fungal spores to the organic carbon and to the aerosol mass balance of the urban atmospheric aerosol, Atmospheric Environment, 42, 5542-5549, 10.1016/j.atmosenv.2008.03.019, 2008.

Bochdansky, A. B., Clouse, M. A., and Herndl, G. J.: Eukaryotic microbes, principally fungi and labyrinthulomycetes, dominate biomass on bathypelagic marine snow, The Isme Journal, 11, 362, 10.1038/ismej.2016.113, 2016.

Bouvier, T., Del Giorgio, P. A., and Gasol, J. M.: A comparative study of the cytometric characteristics of high and low nucleic-acid bacterioplankton cells from different aquatic ecosystems, Environ Microbiol, 9, 2050-2066, 10.1111/j.1462-2920.2007.01321.x, 2007.

Burrows, S. M., Elbert, W., Lawrence, M. G., and Pöschl, U.: Bacteria in the global atmosphere – Part 1: Review and synthesis of literature data for different ecosystems, Atmos. Chem. Phys., 9, 9263-9280, https://doi.org/10.5194/acp-9-9263-2009, 2009.

Chen, P. S., and Li, C. S.: Bioaerosol characterization by flow cytometry with fluorochrome, J Environ Monit, 7, 950-959, 10.1039/b505224f, 2005.

Chi, M.-C., and Li, C.-S.: Fluorochrome in Monitoring Atmospheric Bioaerosols and Correlations with Meteorological Factors and Air Pollutants, Aerosol Science and Technology, 41, 672-678, 10.1080/02786820701383181, 2007.

Comas-Riu, J. and Vives-Rego, J. (2002), Cytometric monitoring of growth, sporogenesis and spore cell sorting in *Paenibacillus polymyxa* (formerly *Bacillus polymyxa*). Journal of Applied Microbiology, 92: 475-481. doi:10.1046/j.1365-2672.2002.01549.x

Crawford, I., Robinson, N. H., Flynn, M. J., Foot, V. E., Gallagher, M. W., Huffman, J. A., Stanley, W. R., and Kaye, P. H.: Characterization of bioaerosol emissions from a Colorado pine forest: results from

915 the BEACHON-RoMBAS experiment, Atmospheric Chemistry and Physics Discussions, 14, 2499-2552,
916 10.5194/acpd-14-2499-2014, 2014.

917 Darrow, L. A., Hess, J., Rogers, C. A., Tolbert, P. E., Klein, M., and Sarnat, S. E.: Ambient pollen
918 concentrations and emergency department visits for asthma and wheeze, Journal of Allergy and Clinical
919 Immunology, 130, 630-638.e634, https://doi.org/10.1016/j.jaci.2012.06.020, 2012.

920 DeLeon-Rodriguez, N., Terry L. Lathem, Luis M. Rodriguez-R, James M. Barazesh, Bruce E. Anderson,
921 Andreas J. Beyersdorf, Luke D. Ziemba, Michael Bergin, Athanasios Nenes, and Konstantinos T.
922 Konstantinidis,: Microbiome of the upper troposphere: Species composition and prevalence, effects of
923 tropical storms, and atmospheric implications, Proceedings of the National Academy of Sciences 110,
924 2575-2580, 2013.

925 DeLeon-Rodriguez, N.: Microbes in the atmosphere: prevalence, species composition, and relevance to
926 cloud formation School of Biology Georgia Institute of Technology, 129 pp.,
927 (http://hdl.handle.net/1853/55517), 2015.

928 Delort, A.-M., and Amato, P.: Microbiology of aerosols, pp.167-168, 2018.

929 Després, V. R., Alex Huffman, J., Burrows, S. M., Hoose, C., Safatov, A. S., Buryak, G., Fröhlich-
930 Nowoisky, J., Elbert, W., Andreae, M. O., Pöschl, U., and Jaenicke, R.: Primary biological aerosol
931 particles in the atmosphere: a review, Tellus B, 64, 10.3402/tellusb.v64i0.15598, 2012.

932 Díaz, M., Herrero, M., García, L. A., and Quirós, C.: Application of flow cytometry to industrial
933 microbial bioprocesses, Biochemical Engineering Journal, 48, 385-407,
934 https://doi.org/10.1016/j.bej.2009.07.013, 2010.

935 Eckenrode, H. M., Jen, S.-H., Han, J., Yeh, A.-G., and Dai, H.-L.: Adsorption of a Cationic Dye Molecule
936 on Polystyrene Microspheres in Colloids: Effect of Surface Charge and Composition Probed by Second
937 Harmonic Generation, The Journal of Physical Chemistry B, 109, 4646-4653, 10.1021/jp045610q, 2005.

938 Elbert, W., Taylor, P. E., Andreae, M. O., & Pöschl, U.: Contribution of fungi to primary biogenic
939 aerosols in the atmosphere: wet and dry discharged spores, carbohydrates, and inorganic ions.,
940 Atmospheric Chemistry and Physics, 7, 4569-4588, 2007.

941 Fröhlich-Nowoisky, J., Kampf, C. J., Weber, B., Huffman, J. A., Pöhlker, C., Andreae, M. O., Lang-
942 Yona, N., Burrows, S. M., Gunthe, S. S., Elbert, W., Su, H., Hoor, P., Thines, E., Hoffmann, T., Després,
943 V. R., and Pöschl, U.: Bioaerosols in the Earth system: Climate, health, and ecosystem interactions,
944 Atmospheric Research, 182, 346-376, http://dx.doi.org/10.1016/j.atmosres.2016.07.018, 2016.

945 Gabey, A. M., Gallagher, M. W., Whitehead, J., Dorsey, J. R., Kaye, P. H., and Stanley, W. R.:
946 Measurements and comparison of primary biological aerosol above and below a tropical forest canopy
947 using a dual channel fluorescence spectrometer, Atmospheric Chemistry and Physics, 10, 4453-4466,
948 10.5194/acp-10-4453-2010, 2010.

949 Gabey, A. M., Stanley, W. R., Gallagher, M. W., and Kaye, P. H.: The fluorescence properties of aerosol
950 larger than 0.8 μm in urban and tropical rainforest locations, Atmospheric Chemistry and Physics, 11,
951 5491-5504, 10.5194/acp-11-5491-2011, 2011.

952 Gosselin, M. I., Rathnayake, C. M., Crawford, I., Pöhlker, C., Fröhlich-Nowoisky, J., Schmer, B.,
953 Després, V. R., Engling, G., Gallagher, M., Stone, E., Pöschl, U., and Huffman, J. A.: Fluorescent

bioaerosol particle, molecular tracer, and fungal spore concentrations during dry and rainy periods in a semi-arid forest, Atmos. Chem. Phys., 16, 15165-15184, 10.5194/acp-16-15165-2016, 2016.

Goudie, A. S.: Desert dust and human health disorders, Environment International, 63, 101-113, http://dx.doi.org/10.1016/j.envint.2013.10.011, 2014.

Griffin, D. W., Kellogg, C. A., Garrison, V. H., Lisle, J. T., Borden, T. C., and Shinn, E. A.: Atmospheric microbiology in the northern Caribbean during African dust events, Aerobiologia, 19, 143-157, 10.1023/B:AERO.0000006530.32845.8d, 2003.

Grote, M., Valenta, R., and Reichelt, R.: Abortive pollen germination: A mechanism of allergen release in birch, alder, and hazel revealed by immunogold electron microscopy, J. Allergy Clin. Immun., 111, 1017–1023, doi:10.1067/mai.2003.1452, 2003.

Guarín, F. A., Abril, M. A. Q., Alvarez, A., and Fonnegra, R.: Atmospheric pollen and spore content in the urban area of the city of Medellin, Colombia, Hoehnea, 42, 9-19, 2015.

Guindulain, T., J. Comas, and J. Vives-Rego: Use of nucleic acid dyes SYTO-13, TOTO-1, and YOYO-1 in the study of Escherichia coli and marine prokaryotic populations by flow cytometry, Applied and environmental microbiology, 63, 4608 - 4611, 1997.

Harrison, R. M., Jones, A. M., Biggins, P. D. E., Pomeroy, N., Cox, C. S., Kidd, S. P., Hobman, J. L., Brown, N. L., and Beswick, A.: Climate factors influencing bacterial count in background air samples, International Journal of Biometeorology, 49, 167-178, 10.1007/s00484-004-0225-3, 2005.

Healy, D. A., Huffman, J. A., O'Connor, D. J., Pöhlker, C., Pöschl, U., and Sodeau, J. R.: Ambient measurements of biological aerosol particles near Killarney, Ireland: a comparison between real-time fluorescence and microscopy techniques, Atmos. Chem. Phys., 14, 8055-8069, 10.5194/acp-14-8055-2014, 2014.

Healy, D. A., O'Connor, D. J., and Sodeau, J. R.: Measurement of the particle counting efficiency of the "Waveband Integrated Bioaerosol Sensor" model number 4 (WIBS-4), Journal of Aerosol Science, 47, 94-99, http://dx.doi.org/10.1016/j.jaerosci.2012.01.003, 2012.

Hernandez, M., Perring, A. E., McCabe, K., Kok, G., Granger, G., and Baumgardner, D.: Chamber catalogues of optical and fluorescent signatures distinguish bioaerosol classes, Atmos. Meas. Tech., 9, 3283-3292, https://doi.org/10.5194/amt-9-3283-2016, 2016.

Hill, S. C., Mayo, M. W., and Chang, R. K.: Fluorescence of bacteria, pollens, and naturally occurring airborne particles: excitation/emission spectra, Army Research Lab Adelphi Md Computational And Information Sciences Directorate, 2009.

Hoose, C., Kristjánsson, J. E., and Burrows, S. M.: How important is biological ice nucleation in clouds on a global scale?, Environmental Research Letters, 5, 024009, 2010.

Hoose, C., and Möhler, O.: Heterogeneous ice nucleation on atmospheric aerosols: a review of results from laboratory experiments, Atmos. Chem. Phys., 12, 9817-9854, 10.5194/acp-12-9817-2012, 2012.

Huffman, J. A., B. Treutlein, and U. Pöschl: Fluorescent biological aerosol particle concentrations and size distributions measured with an Ultraviolet Aerodynamic Particle Sizer (UV-APS) in Central Europe, Atmospheric Chemistry and Physics, 10, 3215-3233, 2010.

992 Huffman, J. A., Prenni, A. J., DeMott, P. J., Pöhlker, C., Mason, R. H., Robinson, N. H., Fröhlich-
993 Nowoisky, J., Tobo, Y., Després, V. R., Garcia, E., Gochis, D. J., Harris, E., Müller-Germann, I., Ruzene,
994 C., Schmer, B., Sinha, B., Day, D. A., Andreae, M. O., Jimenez, J. L., Gallagher, M., Kreidenweis, S. M.,
995 Bertram, A. K., and Pöschl, U.: High concentrations of biological aerosol particles and ice nuclei during
996 and after rain, Atmospheric Chemistry and Physics, 13, 6151-6164, 10.5194/acp-13-6151-2013, 2013.

997 Ingold, C. T.: Fungal spores. Their liberation and dispersal, Oxford, Clarendon Press., 302 pp. pp., 1971.

998 Joly, M., Amato, P., Sancelme, M., Vinatier, V., Abrantes, M., Deguillaume, L., and Delort, A.-M.:
999 Survival of microbial isolates from clouds toward simulated atmospheric stress factors, Atmospheric
1000 Environment, 117, 92-98, https://doi.org/10.1016/j.atmosenv.2015.07.009, 2015.

1001 Joung, Y. S., and Buie, C. R.: Aerosol generation by raindrop impact on soil, 6, 6083,
1002 10.1038/ncomms7083, https://www.nature.com/articles/ncomms7083#supplementary-information, 2015.

1003 Kesavan, J., and Sagripanti, J. L.: Evaluation criteria for bioaerosol samplers, Environ Sci Process
1004 Impacts, 17, 638-645, 10.1039/c4em00510d, 2015.

1005 Lange, J. L. T., P S and Lynch, N: Application of flow cytometry and fluorescent in situ hybridization for
1006 assessment of exposures to airborne bacteria Appl. Environ. Microbiol. , 63, 1557-1563, 1997.

1007 Lebaron, P., Servais, P., Agogue, H., Courties, C., and Joux, F.: Does the high nucleic acid content of
1008 individual bacterial cells allow us to discriminate between active cells and inactive cells in aquatic
1009 systems?, Appl Environ Microbiol, 67, 1775-1782, 10.1128/AEM.67.4.1775-1782.2001, 2001.

1010 Li, D.-W., and Bryce Kendrick: A year-round study on functional relationships of airborne fungi with
1011 meteorological factors, International Journal of Biometeorology 39, 74-80, 1995.

1012 Liang, L., Engling, G., Cheng, Y., Duan, F., Du, Z., and He, K.: Rapid detection and quantification of
1013 fungal spores in the urban atmosphere by flow cytometry, Journal of Aerosol Science, 66, 179-186,
1014 10.1016/j.jaerosci.2013.08.013, 2013.

1015 Lin, H., Gomez, I., and Meredith, J. C.: Pollenkit Wetting Mechanism Enables Species-Specific Tunable
1016 Pollen Adhesion, Langmuir, 29, 3012-3023, 10.1021/la305144z, 2013.

1017 Longo, A. F., Ingall, E. D., Diaz, J. M., Oakes, M., King, L. E., Nenes, A., Mihalopoulos, N., Violaki, K.,
1018 Avila, A., Benitez-Nelson, C. R., Brandes, J., McNulty, I., and Vine, D. J.: P-NEXFS analysis of aerosol
1019 phosphorus delivered to the Mediterranean Sea, Geophysical Research Letters, 41, 4043-4049,
1020 10.1002/2014GL060555, 2014.

1021 Mage, P. L., Csordas, A. T., Brown, T., Klinger, D., Eisenstein, M., Mitragotri, S., Hawker, C., and Soh,
1022 H. T.: Shape-based separation of synthetic microparticles, Nature materials, 18, 82, 2019.

1023 Mathaes, R., Winter, G., Engert, J., and Besheer, A.: Application of different analytical methods for the
1024 characterization of non-spherical micro-and nanoparticles, International journal of pharmaceutics, 453,
1025 620-629, 2013.

1026 Monier, J. M., and Lindow, S. E.: Pseudomonas syringae Responds to the Environment on Leaves by Cell
1027 Size Reduction, Phytopathology, 93, 1209-1216, 10.1094/PHYTO.2003.93.10.1209, 2003.

Morris, C. E., Conen, F., Alex Huffman, J., Phillips, V., Poschl, U., and Sands, D. C.: Bioprecipitation: a feedback cycle linking earth history, ecosystem dynamics and land use through biological ice nucleators in the atmosphere, Glob Chang Biol, 20, 341-351, 10.1111/gcb.12447, 2014.

Muller, S., and Nebe-von-Caron, G.: Functional single-cell analyses: flow cytometry and cell sorting of microbial populations and communities, FEMS Microbiol Rev, 34, 554-587, 10.1111/j.1574-6976.2010.00214.x, 2010.

Myriokefalitakis, S., Nenes, A., Baker, A. R., Mihalopoulos, N., and Kanakidou, M.: Bioavailable atmospheric phosphorous supply to the global ocean: a 3-D global modeling study, Biogeosciences, 13, 6519-6543, 10.5194/bg-13-6519-2016, 2016.

Nir, R., Yisraeli, Y., Lamed, R., & Sahar, E.: Flow cytometry sorting of viable bacteria and yeasts according to beta-galactosidase activity, Applied and environmental microbiology, 56, 3861-3866, 1990.

Oliveira, M., Ribeiro, H., Delgado, J. L., and Abreu, I.: The effects of meteorological factors on airborne fungal spore concentration in two areas differing in urbanisation level, Int J Biometeorol, 53, 61-73, 10.1007/s00484-008-0191-2, 2009.

Ortiz-Martínez, Mario G., Rosa I. Rodríguez-Cotto, Mónica A. Ortiz-Rivera, Cedric W. Pluguez-Turull, and Braulio D. Jiménez-Vélez. Linking endotoxins, African dust PM10 and asthma in an urban and rural environment of Puerto Rico. *Mediators of inflammation* 2015.

Pan, Y.-L., Santarpia, J. L., Ratnesar-Shumate, S., Corson, E., Eshbaugh, J., Hill, S. C., Williamson, C. C., Coleman, M., Bare, C., and Kinahan, S.: Effects of ozone and relative humidity on fluorescence spectra of octapeptide bioaerosol particles, Journal of Quantitative Spectroscopy and Radiative Transfer, 133, 538-550, https://doi.org/10.1016/j.jqsrt.2013.09.017, 2014.

Perring, A. E., et al. (2015), Airborne observations of regional variation in fluorescent aerosol across the United States, *J. Geophys. Res. Atmos.*, 120, 1153–1170, doi:10.1002/2014JD022495.

Pöhlker, C., Huffman, J. A., Förster, J. D., and Pöschl, U.: Autofluorescence of atmospheric bioaerosols: spectral fingerprints and taxonomic trends of pollen, Atmospheric Measurement Techniques, 6, 3369-3392, 10.5194/amt-6-3369-2013, 2013.

Pöhlker, C., Huffman, J. A., and Pöschl, U.: Autofluorescence of atmospheric bioaerosols – fluorescent biomolecules and potential interferences, Atmospheric Measurement Techniques, 5, 37-71, 10.5194/amt-5-37-2012, 2012.

Pöschl, U.: Atmospheric Aerosols: Composition, Transformation, Climate and Health Effects, Angewandte Chemie International Edition, 44, 7520-7540, 10.1002/anie.200501122, 2005.

Robinson, N. H., Allan, J. D., Huffman, J. A., Kaye, P. H., Foot, V. E., and Gallagher, M.: Cluster analysis of WIBS single-particle bioaerosol data, Atmos. Meas. Tech., 6, 337-347, https://doi.org/10.5194/amt-6-337-2013, 2013.

Rödiger, S., Ruhland, M., Schmidt, C., Schröder, C., Grossmann, K., Böhm, A., Nitschke, J., Berger, I., Schimke, I., and Schierack, P.: Fluorescence Dye Adsorption Assay to Quantify Carboxyl Groups on the Surface of Poly(methyl methacrylate) Microbeads, Analytical Chemistry, 83, 3379-3385, 10.1021/ac103277s, 2011.

S.-L.Von der Weiden, F. D., and S. Borrmann: Particle Loss Calculator - a new software tool for the assessment of the performance of aerosol inlet systems, Atmospheric Measurement Techniques, 2, 479-494, 2009.

Saari, S., Reponen, T., and Keskinen, J.: Performance of Two Fluorescence-Based Real-Time Bioaerosol Detectors: BioScout vs. UVAPS, Aerosol Science and Technology, 48, 371-378, 10.1080/02786826.2013.877579, 2014.

Šantl-Temkiv, T., Amato, P., Gosewinkel, U., Thyrhaug, R., Charton, A., Chicot, B., Finster, K., Bratbak, G., and Löndahl, J.: High-Flow-Rate Impinger for the Study of Concentration, Viability, Metabolic Activity, and Ice-Nucleation Activity of Airborne Bacteria, Environmental Science & Technology, 51, 11224-11234, 10.1021/acs.est.7b01480, 2017.

Savage, N. J., Krentz, C. E., Könemann, T., Han, T. T., Mainelis, G., Pöhlker, C., and Huffman, J. A.: Systematic characterization and fluorescence threshold strategies for the wideband integrated bioaerosol sensor (WIBS) using size-resolved biological and interfering particles, Atmospheric Measurement Techniques, 10, 4279-4302, 10.5194/amt-10-4279-2017, 2017.

Shapiro, Howard M. Practical flow cytometry. John Wiley & Sons, 2005.

Standaert-Vitse, A., Aliouat-Denis, C.-M., Martinez, A., Khalife, S., Pottier, M., Gantois, N., Dei-Cas, E., and Aliouat, E. M.: SYTO-13, a Viability Marker as a New Tool to Monitor In Vitro Pharmacodynamic Parameters of Anti-Pneumocystis Drugs, PLoS One, 10, e0130358-e0130358, 10.1371/journal.pone.0130358, 2015.

Sullivan, S. C., Hoose, C., Kiselev, A., Leisner, T., and Nenes, A.: Initiation of secondary ice production in clouds, Atmos. Chem. Phys. Discuss., 2017, 1-22, 10.5194/acp-2017-387, 2017.

Taylor, P. E., Jacobson, K. W., House, J. M., and Glovsky, M. M.: Links between pollen, atopy and the asthma epidemic, Int Arch Allergy Immunol, 144, 162-170, 10.1159/000103230, 2007.

Toprak, E., and Schnaiter, M.: Fluorescent biological aerosol particles measured with the Waveband Integrated Bioaerosol Sensor WIBS-4: laboratory tests combined with a one year field study, Atmospheric Chemistry and Physics, 13, 225-243, 10.5194/acp-13-225-2013, 2013.

Troussellier, M., Courties, C., Lebaron, P., and Servais, P.: Flow cytometric discrimination of bacterial populations in seawater based on SYTO 13 staining of nucleic acids, FEMS Microbiology Ecology, 29, 319-330, https://doi.org/10.1016/S0168-6496(99)00026-4, 1999.

Tzur A, Moore JK, Jorgensen P, Shapiro HM, Kirschner MW (2011) Optimizing Optical Flow Cytometry for Cell Volume-Based Sorting and Analysis. PLoS ONE 6(1): e16053. https://doi.org/10.1371/journal.pone.0016053

Van Dilla, M. A., Langlois, R. G., Pinkel, D., Yajko, D., & Hadley, W. K.: Bacterial characterization by flow cytometry., Science, 220, 620-622, 1983.

Wang, Y., Hammes, F., De Roy, K., Verstraete, W., and Boon, N.: Past, present and future applications of flow cytometry in aquatic microbiology, Trends Biotechnol, 28, 416-424, 10.1016/j.tibtech.2010.04.006, 2010.

Wu, Y.-H., Chan, C.-C., Rao, C. Y., Lee, C.-T., Hsu, H.-H., Chiu, Y.-H., and Chao, H. J.: Characteristics, determinants, and spatial variations of ambient fungal levels in the subtropical Taipei metropolis, Atmospheric Environment, 41, 2500-2509, 10.1016/j.atmosenv.2006.11.035, 2007.

Yu, X., Wang, Z., Zhang, M., Kuhn, U., Xie, Z., Cheng, Y., Pöschl, U., and Su, H.: Ambient measurement of fluorescent aerosol particles with a WIBS in the

Yangtze River Delta of China: potential impacts of combustion-related aerosol particles, Atmospheric Chemistry and Physics, 16, 11337-11348, 10.5194/acp-16-11337-2016, 2016.

Yue, S., Ren, H., Fan, S., Sun, Y., Wang, Z., and Fu, P.: Springtime precipitation effects on the abundance of fluorescent biological aerosol particles and HULIS in Beijing, Sci Rep, 6, 29618, 10.1038/srep29618, 2016.

Yue, S., Ren, H., Fan, S., Wei, L., Zhao, J., Bao, M., Hou, S., Zhan, J., Zhao, W., Ren, L., Kang, M., Li, L., Zhang, Y., Sun, Y., Wang, Z., and Fu, P.: High Abundance of Fluorescent Biological Aerosol Particles in Winter in Beijing, China, ACS Earth and Space Chemistry, 1, 493-502, 10.1021/acsearthspacechem.7b00062, 2017.

Zhen, H., Han, T., Fennell, D. E., and Mainelis, G.: Release of free DNA by membrane-impaired bacterial aerosols due to aerosolization and air sampling, Appl Environ Microbiol, 79, 7780-7789, 10.1128/AEM.02859-13, 2013.

Ziemba, L. D., Beyersdorf, A. J., Chen, G., Corr, C. A., Crumeyrolle, S. N., Diskin, G., Hudgins, C., Martin, R., Mikoviny, T., Moore, R., Shook, M., Thornhill, K. L., Winstead, E. L., Wisthaler, A., and Anderson, B. E.: Airborne observations of bioaerosol over the Southeast United States using a Wideband Integrated Bioaerosol Sensor, Journal of Geophysical Research: Atmospheres, 121, 8506-8524, 10.1002/2015JD024669, 2016.

Table 1: Summary of the SpinCon II sampling events, the 24 h. averaged RH, ambient temperature, the assigned meteorological category (using Section 4.4 definitions) and the corrected FCM-derived PBAP number concentration (1 to 5 µm) for each sample collected during this study.

Date (starting – ending time)	RH (%)	Temperature (°C)	Meteorological Category	PBAP Concentration (m^{-3}) 1 to 5µm diameter range
4/7/15 (11:17 - 15:17) *	70.9	21.4	Humid, Warm	9.282×10^{4}
4/8/15 (11:10 - 15:10)	53.6	24.9	Dry, Warm	5.203×10^{5}
4/9/15 (11:15 - 15:15)	53.8	25.3	Dry, Warm	1.254×10^{5}
4/14/15 (11:30 - 15:30) *	76.8	22.5	Humid, Warm	8.253×10^{4}
4/15/15 (11:40 - 15:40) *	83.6	18.9	Humid, Warm	1.234×10^{5}
4/16/15 (10:55 - 14:55)	86.3	12.5	Humid, Cold	3.399×10^{5}
4/21/15 (13:15 - 17:15)	43.2	16.6	Dry, Cold	4.741×10^{5}
4/22/15 (11:25 - 15:25)	38.1	18.8	Dry, Warm	3.351×10^{5}
4/23/15 (11:35 - 15:35)	48.1	16.8	Dry, Cold	1.708×10^{6}
4/28/15 (12:25 - 16:25)	45.3	17.0	Dry, Cold	4.899×10^{5}
4/29/15 (11:55 - 15:55) #	79.4	14.2	Humid, Cold	4.591×10^{5}
4/30/15 (12:10 - 16:10)	57.3	17.4	Dry, Cold	9.603×10^{5}
5/13/15 (10:50 - 14:50)	40.1	23.5	Dry, Warm	3.680×10^{5}
5/14/15 (11:50 - 15:50)	52.3	23.0	Dry, Warm	4.851×10^{5}
5/15/15 (10:19 - 14:19)	64.4	23.1	Dry, Warm	1.656×10^{6}

* Sampling occurred post-rain event.
# Sampling occurred during a rain event.

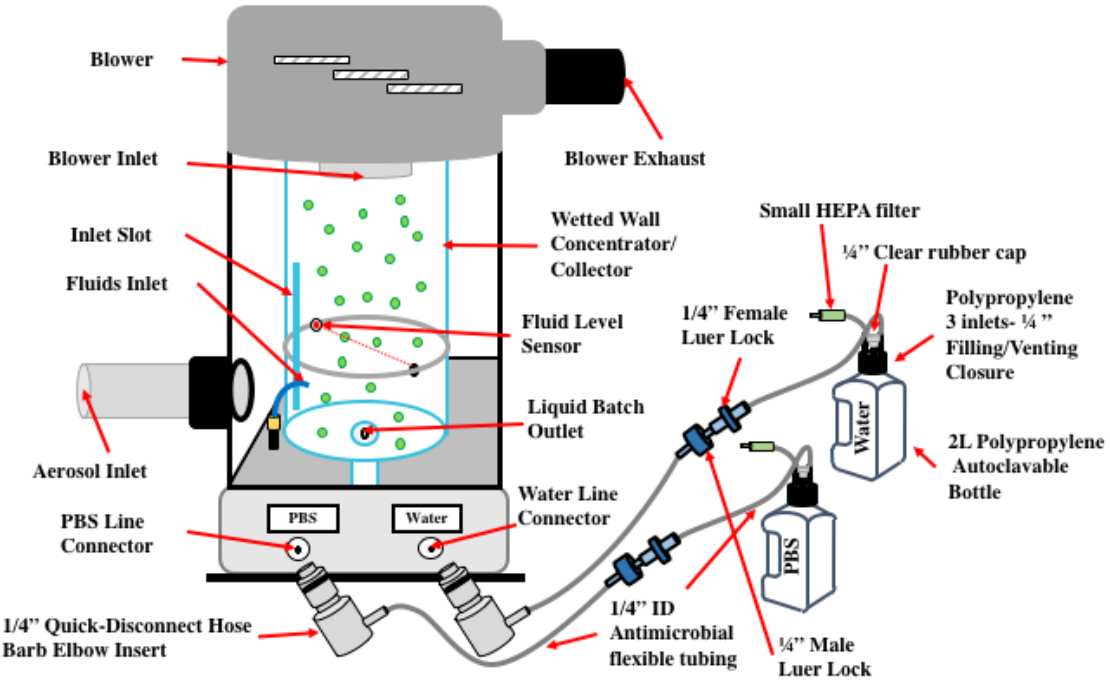

Figure 1: SpinCon II sampling setup including modified fluid supply system with anti-microbial tubing and 2L Autoclavable bottles.

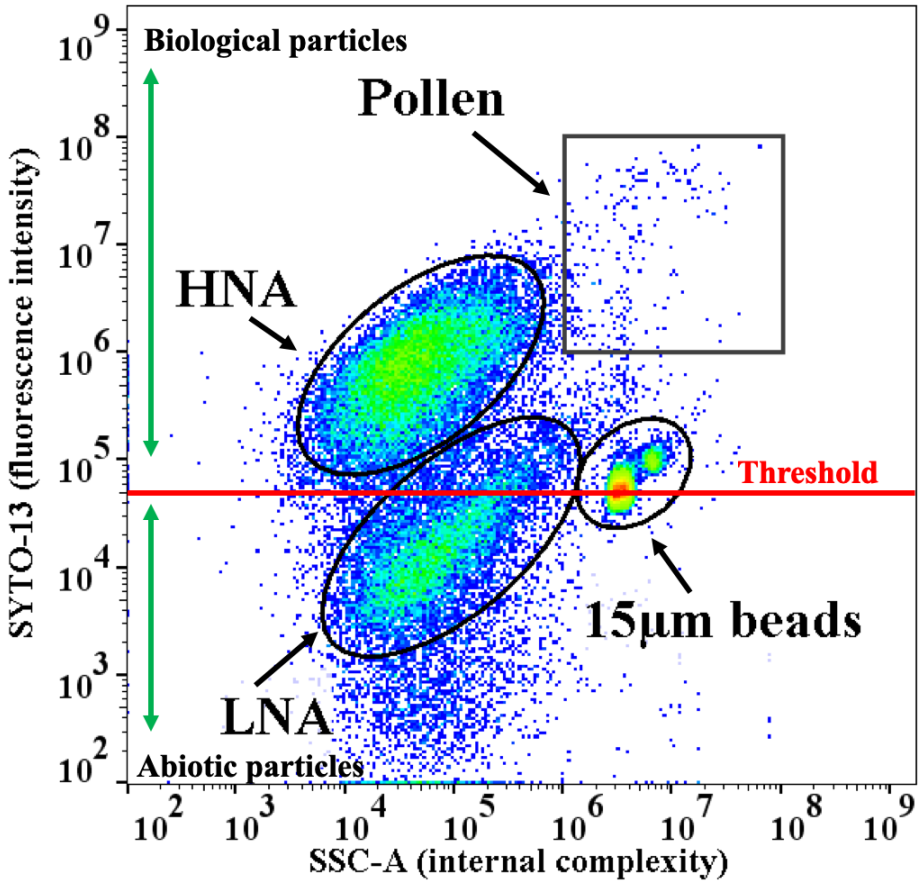

Figure 2: FL1-A vs. SSC-A plot used to identify populations in the April 14, 2015 sample including: the 42k threshold line in red and, abiotic particles (below threshold) and biological particles (above threshold) designated regions. In the density plot green and red zones denote the most populated regions. FL1-A in the y-axis shows the fluorescence intensity of each particle in the plot stained with SYTO-13 and SSC-A in the x-axis measures 90° light scattering, related to the internal complexity (e.g. granularity or amount of internal structures) and size of the particles. The fraction of the LNA population above the threshold line is referred as the "LNA-AT" population.

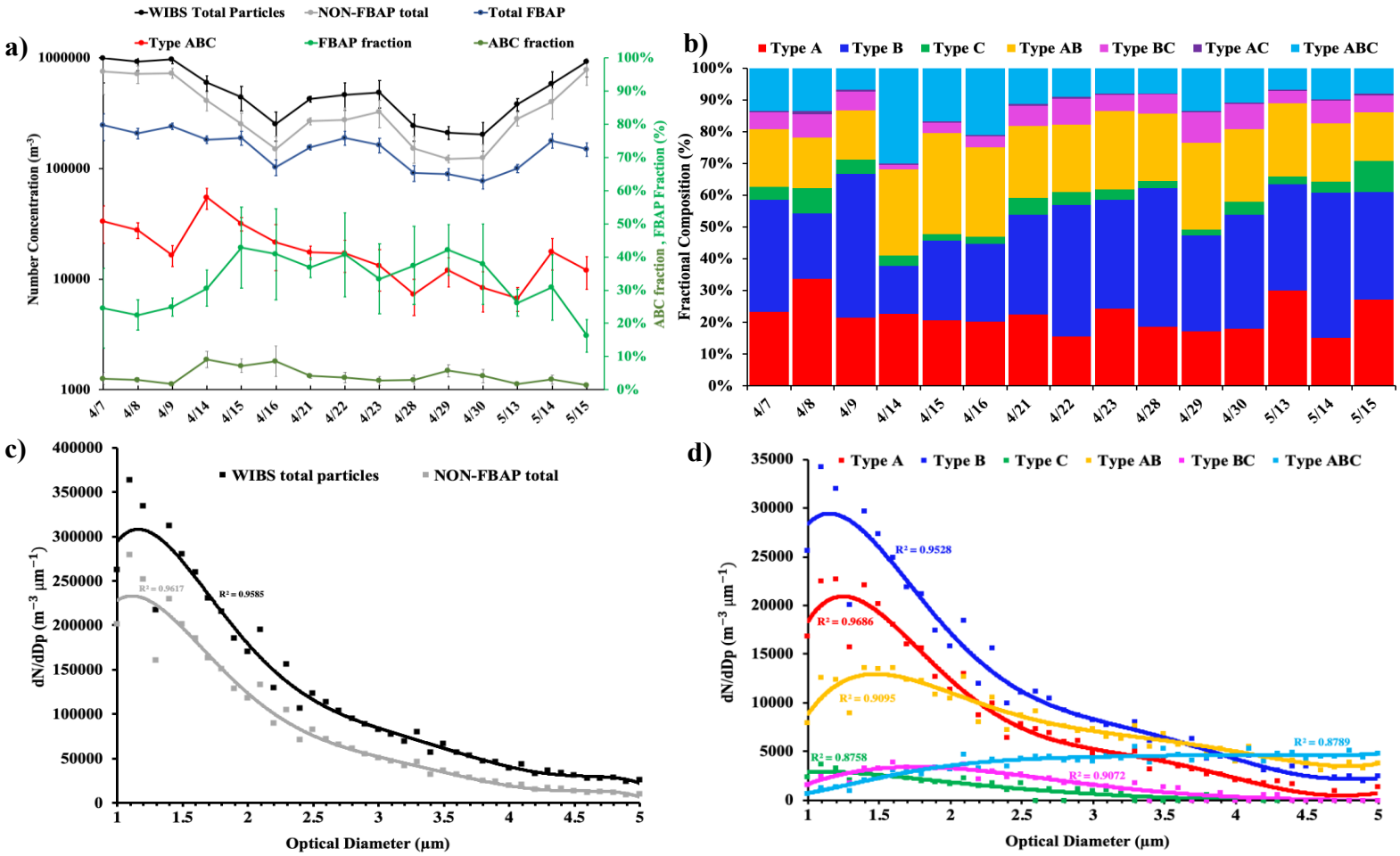

Figure 3: WIBS-4A 4hr (SpinCon II sampling time) averaged results of WIBS total particle, NON-FBAP, total FBAP and type ABC concentrations in the left Y-axis and ABC and FBAP fraction in the right Y-axis for each SpinCon II sampling event in (a); 4hr averaged FBAP types number concentration fractional composition for each SpinCon II sampling event in (b); 1to5µm WIBS total particles and NON-FBAP size distributions in (c) and 1to5µm size distributions for all FBAP types, except AC type in (d). AC type showed low statistics and constituted less than 1% of the total FBAP (not shown). Size distributions in (c) and (d) have been averaged over the 15 SpinCon II sampling events and constitute the overall size distributions during rooftop sampling events. Solid lines in (c) and (d) shown 6-degree polynomial regressions performed to FBAP the size distributions, including their respective correlation coefficients (R^2).

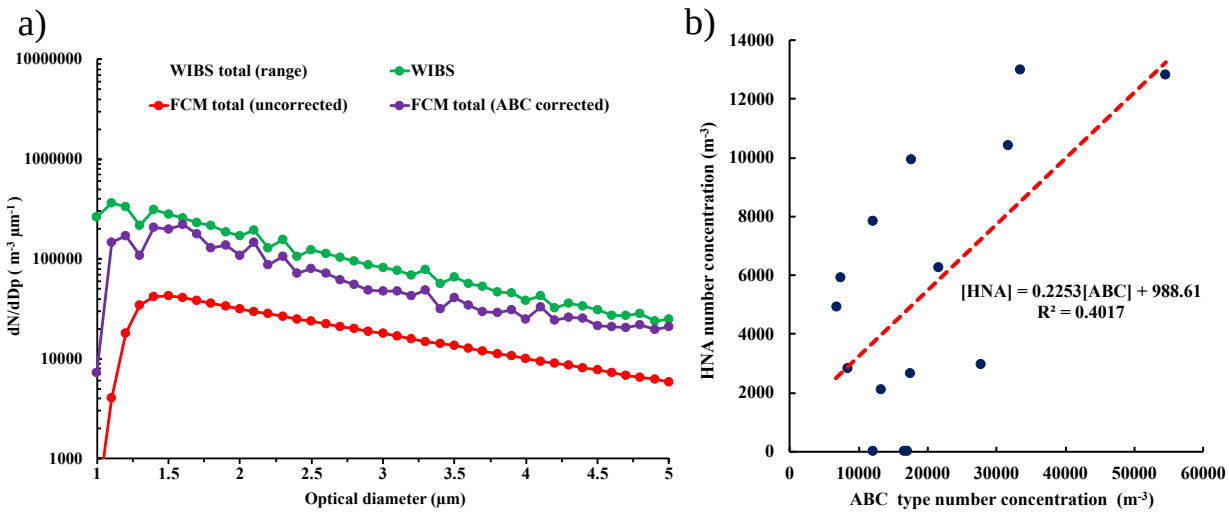

Figure 4: WIBS-4A, FCM uncorrected and FCM (ABC corrected) total particle concentration (1 to 5µm) average size distributions (geometrically averaged over the 15 SpinCon II sampling events) including WIBS range (± geometric standard deviation factor) in (a); and HNA and ABC type concentration correlation in the 1 to 5µm range in (b) including it linear correlation in red.

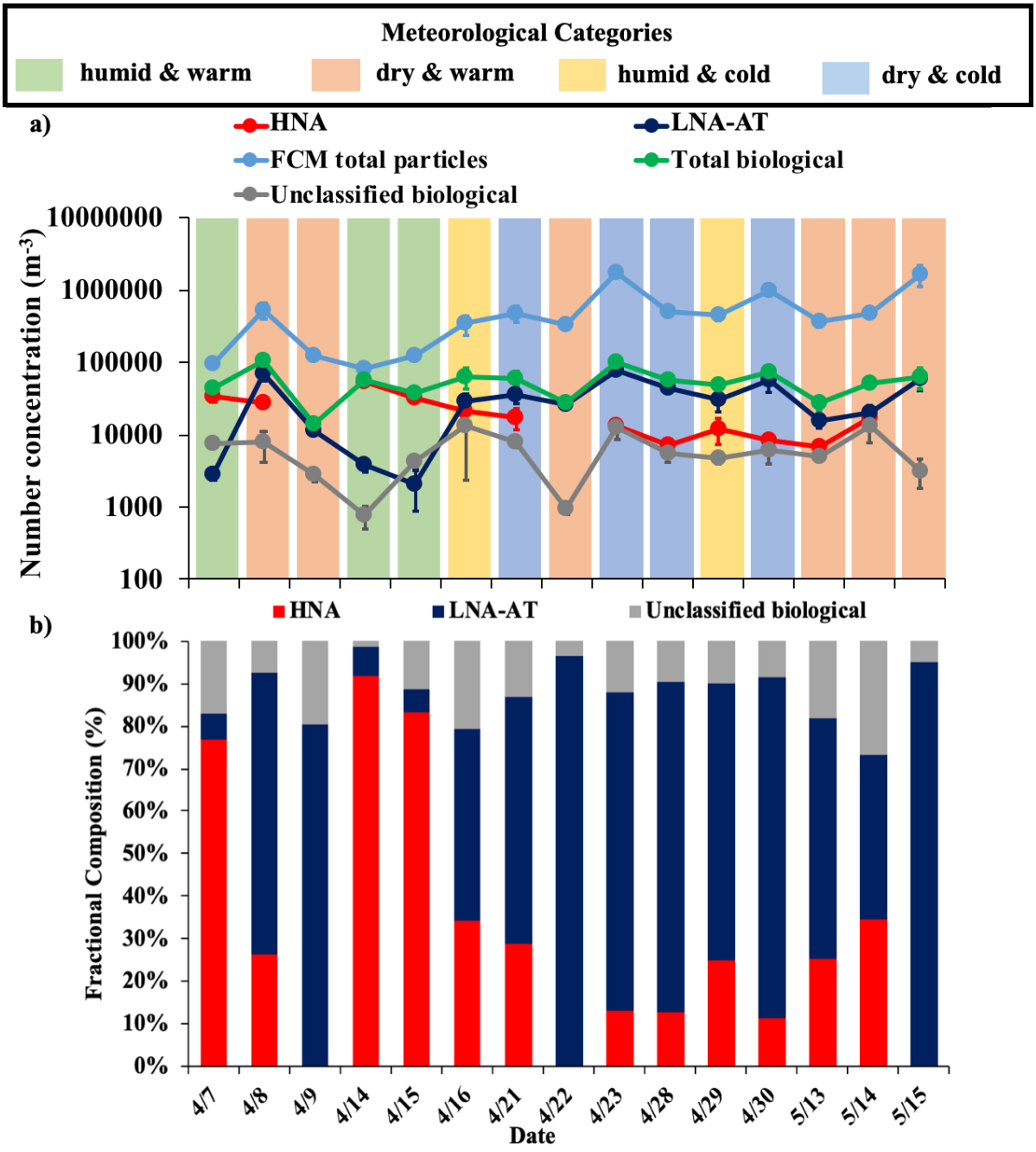

Figure 5: FCM total particle, HNA, LNA-AT and total PBAP number concentrations in the 1 to 5µm range highlighting the prevailing meteorological category during each sampling event in (a); HNA and LNA-AT number concentration fractional compositions for each sampling event in (b).

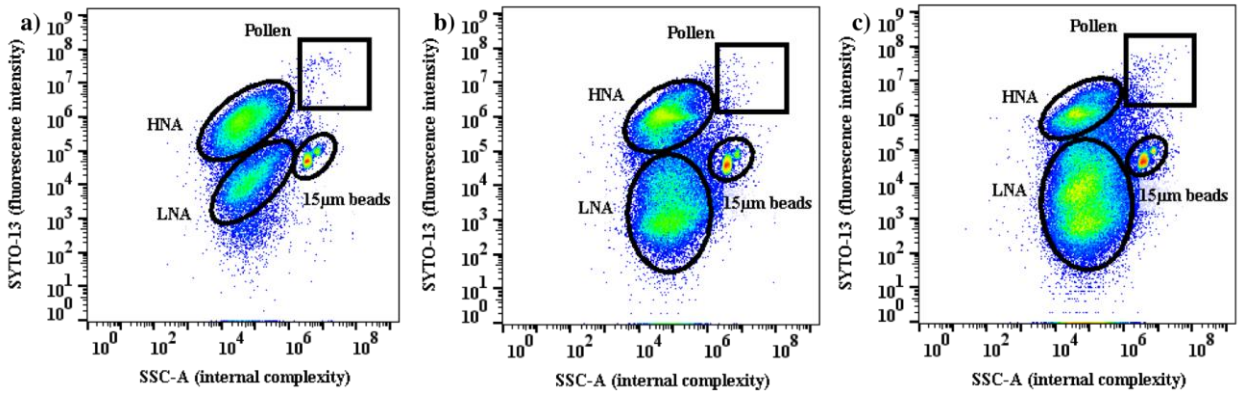

Figure 6: FL1-A vs. SSC-A FSC plots for (a) April 14, (b) April 15, and, (c) April 16. This period was characterized by a transition from humid & warm to humid & cold conditions (diurnal average RH=77%, T=22.5 ºC on 4/14; RH=84%, T=18.9 ºC on 4/15, and RH= 86%, T= 12.5 ºC on 4/16). The FCM plots during this transition period show a decrease of fungal population and an increase of the LNA population. In each population, warmer colors represent higher particle concentrations.

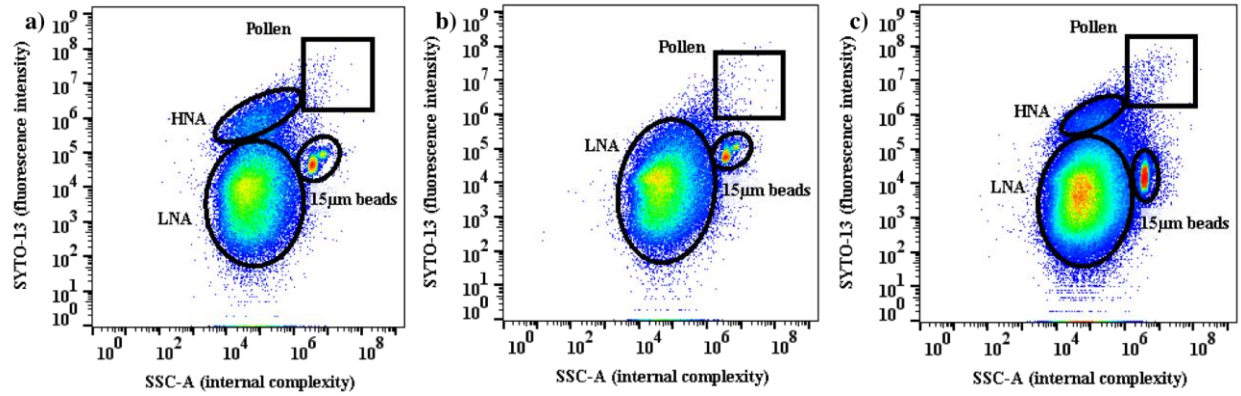

Figure 7: Similar to Figure 6, but for (a) April 21, (b) April 22, (c) April 23, which was characterized by dry and variability in temperature (diurnal average RH=43%, T=16.6 ºC on 4/21; RH=41%, T=19.0 ºC on 4/22, and, RH= 48%, T= 16.8 ºC on 4/23. Note the disappearance of the fungal spore population on the warmest day (4/22).

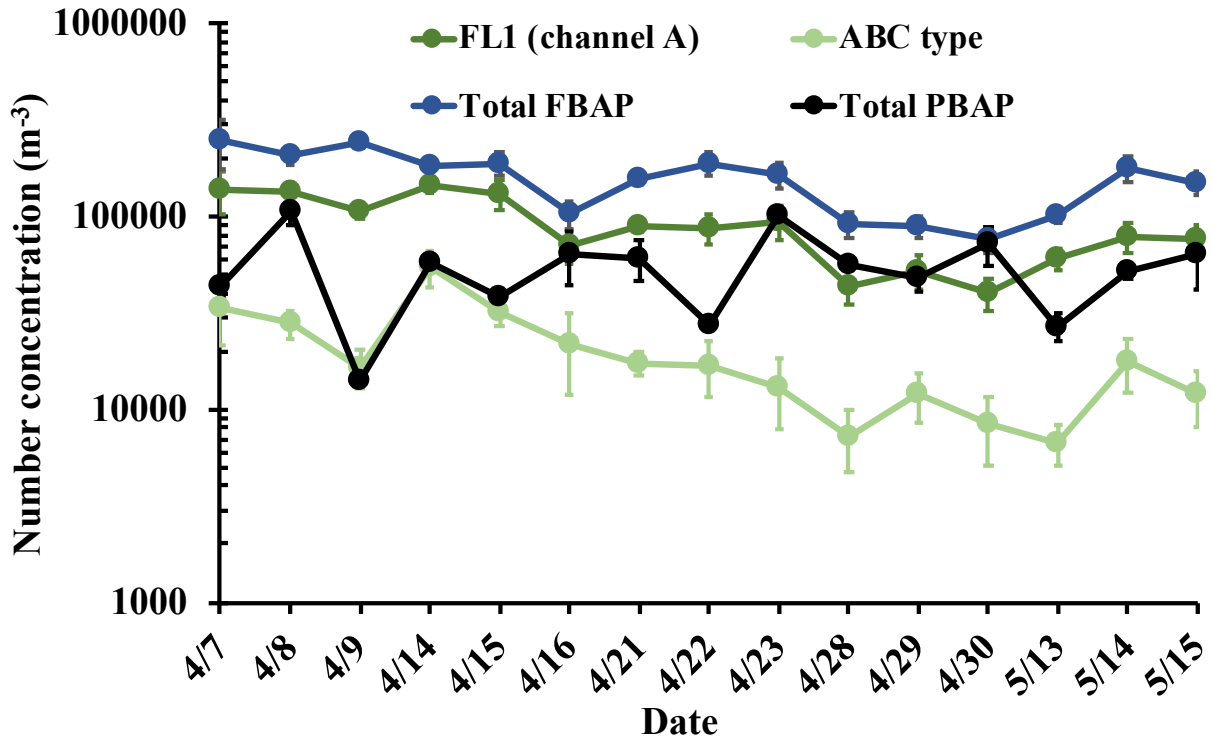

Figure 8: WIBS-4A total FBAP, FL1 and ABC type, and FCM total particle number concentrations in the 1 to 5µm range for each sampling event from April 7 to May 15, 2015.